

UCRL-96816
PREPRINT

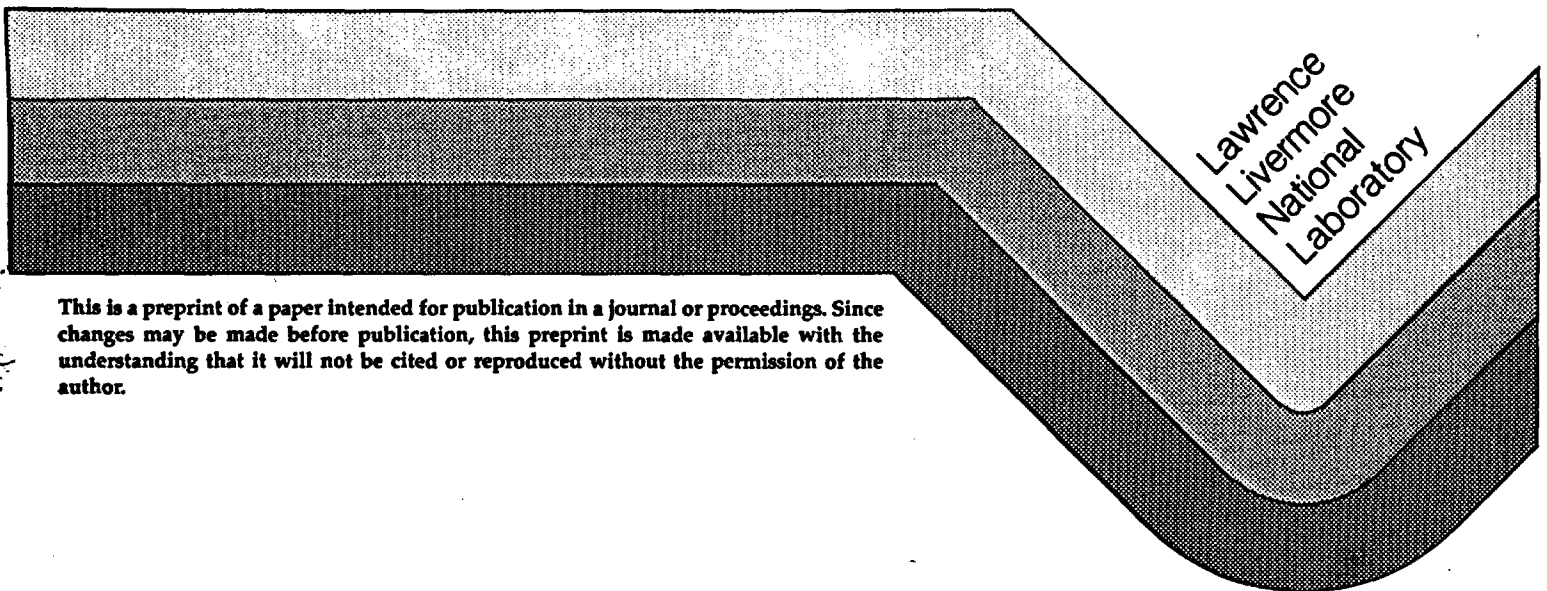
PRELIMINARY EVALUATION OF AN ELECTROMAGNETIC
EXPERIMENT TO MAP IN SITU WATER IN
HEATED WELDED TUFF

William D. Daily
Abelardo L. Ramirez

HYDROLOGY DOCUMENT NUMBER 97

This paper was prepared for submittal to
IEEE Geoscience and Remote Sensing

February 1987



This is a preprint of a paper intended for publication in a journal or proceedings. Since changes may be made before publication, this preprint is made available with the understanding that it will not be cited or reproduced without the permission of the author.

DISCLAIMER

This document was prepared as an account of work sponsored by an agency of the United States Government. Neither the United States Government nor the University of California nor any of their employees, makes any warranty, express or implied, or assumes any legal liability or responsibility for the accuracy, completeness, or usefulness of any information, apparatus, product, or process disclosed, or represents that its use would not infringe privately owned rights. Reference herein to any specific commercial products, process, or service by trade name, trademark, manufacturer, or otherwise, does not necessarily constitute or imply its endorsement, recommendation, or favoring by the United States Government or the University of California. The views and opinions of authors expressed herein do not necessarily state or reflect those of the United States Government or the University of California, and shall not be used for advertising or product endorsement purposes.

ABSTRACT

An experiment was conducted in Tunnel Complex G at the Nevada Test Site to evaluate geotomography as a possible candidate for in situ monitoring of moisture content near a simulated nuclear waste container placed in densely welded tuff. Alterant tomographs of 200 MHz electromagnetic permittivity were made in the densely welded tuff in two planes near a heater. When the 1 kilowatt heater was turned on the tomographs indicated a rapid and strong drying adjacent to the heater. Moisture loss was not symmetric about the heater but seemed to be strongly influenced by heterogeneity in the rock mass. The linear character of many tomographic features and their spatial correlation with fractures mapped in boreholes are evidence that drying was most rapid along certain fractures. When the heater was turned off an increase in moisture content occurred around the heater and along the dry lineaments. However, this process is much slower and the magnitude of the moisture increase much smaller than the changes observed during heating of the rock. The interpretation of the tomographs is preliminary until they can be processed without the restrictive assumption of straight ray paths for the signals through the highly heterogeneous rock mass. However, from these preliminary results we conclude that geotomography can provide useful moisture content information near a heater in densely welded tuff. This conclusion is based on the fact that the experiment results and their interpretation are self consistent and in good agreement with behavior expected of the heated rock mass.

1. INTRODUCTION

The Nevada Nuclear Waste Storage Investigations (NNWSI) Project is studying the suitability of the tuffaceous rocks at Yucca Mountain, Nevada Test Site, for the construction of a high-level nuclear waste repository. Lawrence Livermore National Laboratory (LLNL), Livermore, California, has been given the task of designing and assessing the performance of waste packages for the NNWSI Project.

The properties of the geologic environment around a waste package must be well characterized so that performance can be reliably assessed. Many factors controlling the properties of the geologic environment are strongly interrelated. The heat generated by a waste package will disturb the adjacent rock mass. Groundwater (steam where the temperatures are sufficiently high) will move through the fractures and pores thereby changing the physical and chemical properties of the rock mass. These changes may impact the performance of a waste package.

Various in-situ tests will be conducted within the Topopah Spring member of the Paintbrush Tuff at Yucca Mountain to investigate rock mass behavior in the vicinity of simulated waste packages. The planned tests will simulate the environment near the waste packages by emplacement of heaters within the rock mass. Rock behavior will be monitored during the heating and cooling phases and with water percolating through the rock mass. A key objective of this work is to study the hydrologic behavior of the rock under a thermal load.

The interaction of groundwater and rock surrounding the simulated waste package will be studied with various measurement techniques. This report discusses the results of an experiment in which one of the candidate

measurement techniques, alterant geophysical tomography (Ramirez and Lytle, 1986; Ramirez and Daily, 1987) was used to detect changes in moisture content created by a heater in welded tuff. The objective of the experiment was to evaluate the capability of alterant geophysical tomography to map the changes in moisture content occurring within a few meters of the heater location. A description of the tomographic reconstruction technique is provided in Appendix A. Other heater experiments conducted at G-Tunnel are described by Zimmerman (1983), and Zimmerman, et al. (1984).

The hydrologic environment expected to develop around a heater is shown schematically in Fig. 1. The heater will dry the partially saturated rock near the emplacement borehole. The water vapor formed will be driven by vapor pressure gradients through the matrix until it intersects a fracture and then move along the fracture. Laboratory work performed by Daily, et al. (1987) suggests that this expected drying mechanism is viable. The water vapor will condense where the temperatures are sufficiently cool. Part of this water may move into the matrix due to capillary tension while the remainder may remain in the fracture held by capillarity or it may flow along the fracture under gravity. When the dried region is allowed to cool it may be expected to slowly rewet.

2. EXPERIMENT DESCRIPTION

2.1. ALTERANT GEOPHYSICAL TOMOGRAPHY

Geophysical tomography is similar conceptually to the medical tomography which inspired it (Kuhl and Edwards, 1963 and Lager and Lytle, 1977). A

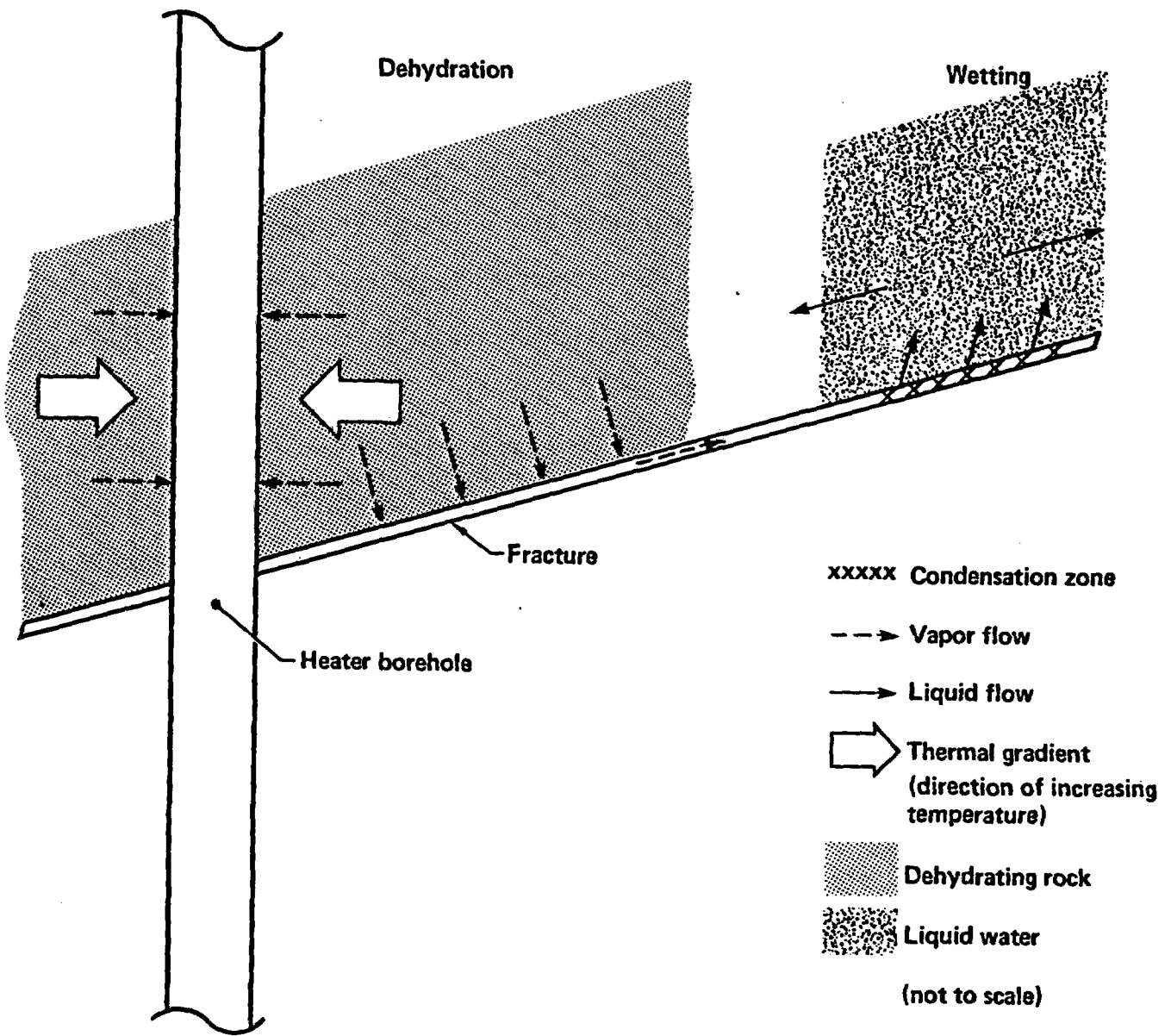


Figure 1. Schematic representation of a possible hydrologic scenario in partially saturated, welded tuff subjected to a thermal load.

region to be studied is sampled by transmitting energy through it along many paths having varied orientations, and from the properties of this transmission data a cross-sectional image of the region is inferred. For this study, measurements of very high frequency electromagnetic energy (185-215 MHz) were used because rock mass electromagnetic properties depend strongly on (among other things) water content of the rock (Poley, et al., 1978; Daily and Ramirez, 1984; Hearst and Nelson, 1985). The complex electromagnetic permittivity of the rock is defined as

$$\epsilon = \epsilon_r - j\epsilon_i$$

$$\text{where } j = \sqrt{-1}$$

For a homogeneous material the real part ϵ_r corresponds to the dipolar, ionic and electronic polarizability and is usually called the dielectric constant. The imaginary part, ϵ_i , corresponds to energy dissipation in the rock due to dipole rotation and motion of free charge carriers. The complex permittivity of the rock depends on the permittivities of its two basic constituents: silicate matrix and water. For the rock matrix, at the frequency of interest, $\epsilon_r \sim 2-4 \epsilon_0$ but for the water $\epsilon_r \sim 80 \epsilon_0$ (Von Hippel, 1954). It is this large contrast that makes the real part of the permittivity for rock a valuable diagnostic of its water content. Small changes in water content can result in measurable changes in ϵ_r for the rock mass. Wave equations describing a propagating wave of angular frequency ω are governed by the propagation constant

$$\gamma = j\omega (\epsilon\mu)^{1/2}$$

where ϵ and μ are the complex EM permittivity and complex EM permeability, respectively, of the medium. In the nonmagnetic case, as for the rock of interest in this study, $\mu = \mu_0$ where μ_0 is the magnetic permeability of free space. Note that the imaginary part of the magnetic permeability is assumed negligible. Then $\gamma = j\omega (\epsilon\mu_0)^{1/2} = \alpha + j\beta$ and for the case where $\epsilon_i/\epsilon_r \ll 1$ the phase factor $\beta = \omega (\epsilon_r\mu_0)^{1/2}$. The phase change ϕ of an electromagnetic wave traveling a distance R is

$$\phi = \beta R$$

which can be written as

$$\phi = \omega R (\epsilon_r)^{1/2} / c$$

where c is the speed of the wave in free space. By changing the frequency of the plane wave from ω_1 to ω and noting the phase change, it is possible to obtain the dielectric constant of the transmission medium

$$(\epsilon_r)^{1/2} = \frac{c}{R} \frac{\Delta\phi}{\Delta\omega}$$

where $\Delta\omega = \omega_2 - \omega_1$ and $\Delta\phi = \phi(\omega_2) - \phi(\omega_1)$.

off. These alterant tomographs should delineate water content changes, relative to the driest state in the rock mass, as the thermal field collapses and water is moved by capillarity and gravity back into the tomographic plane.

Some of the procedures and instrumentation which we expected to use at G-tunnel required testing prior to the experiment. These tests were conducted in a large pit filled with sand in which anomalies were buried to electromagnetically simulate a fracture and a dehydrated zone. The sand pit test and results affecting the field experiment design are discussed in Appendix B.

2.2. GEOLOGIC SETTING

The experiment was conducted in G-Tunnel at the Department of Energy, Nevada Test Site, Nye County, Nevada. This tunnel provides access to a welded ash flow tuff formation of the Grouse Canyon member of the Belted Range Tuff. This formation was of interest because it has similar properties to the proposed repository horizon, the Topopah Spring tuff, at Yucca Mountain. It has been established that the welded tuffs in G-Tunnel have similar bulk, thermal and mechanical properties to those at Yucca Mountain (Zimmerman, et al., 1984). The Grouse Canyon tuff exposed in G-Tunnel is a partially to densely welded tuff striking N55°E and dipping 9°W. This formation is in the unsaturated zone but has a degree of saturation greater than 60% and a porosity ranging from 15 to 46% as reported by Zimmerman and Blanford (1986). For the same formation Johnstone and Wolfsberg (1980) report a porosity ranging from 13 to 25 percent and a saturation greater than 85%.

2.3. BOREHOLE CONFIGURATION

Measurements were made between a series of horizontal boreholes drilled into the rib of the small diameter heater alcove and perpendicular to the heater hole which was drilled from the tunnel (Fig. 2). Three of the boreholes (A, B and D) define two planes (AB and BD) in the rock mass which were sampled for tomographic reconstruction; each plane was two meters long and one meter wide. Both measurement planes were at least 3.4 meters from a tunnel rib. Measurement plane AB was vertical with the heater borehole E, intersecting it at a nearly perpendicular angle. The other tomographic plane was nearly parallel to, and about 1/2 meter from, the heater axis. Another borehole (C), drilled to dip a few degrees below horizontal, was used to introduce distilled water to the fracture systems which it intersected.

2.4. DATA COLLECTION

The experiment was more than three months in duration. Figure 3 outlines the sequence of data acquisition relative to heating and cooling of the rock mass. Initially, tomographs were made of measurement planes B-A (vertical) and B-D (horizontal), and neutron logs were run in holes A, B and E. (Blocks of rock were falling into borehole D requiring that it be cased. This precluded use of the neutron probe in borehole D.) The heater was turned on April 29th in borehole E and heater power was adjusted to one kilowatt electrical. During the 34 days of heating, E.M. tomographic data and neutron logs were taken as indicated in Fig. 3. During four days water was introduced to the rock mass from borehole C at a rate of roughly two gallons per hour. The heater was then turned off and tomographs and neutron logs taken as the

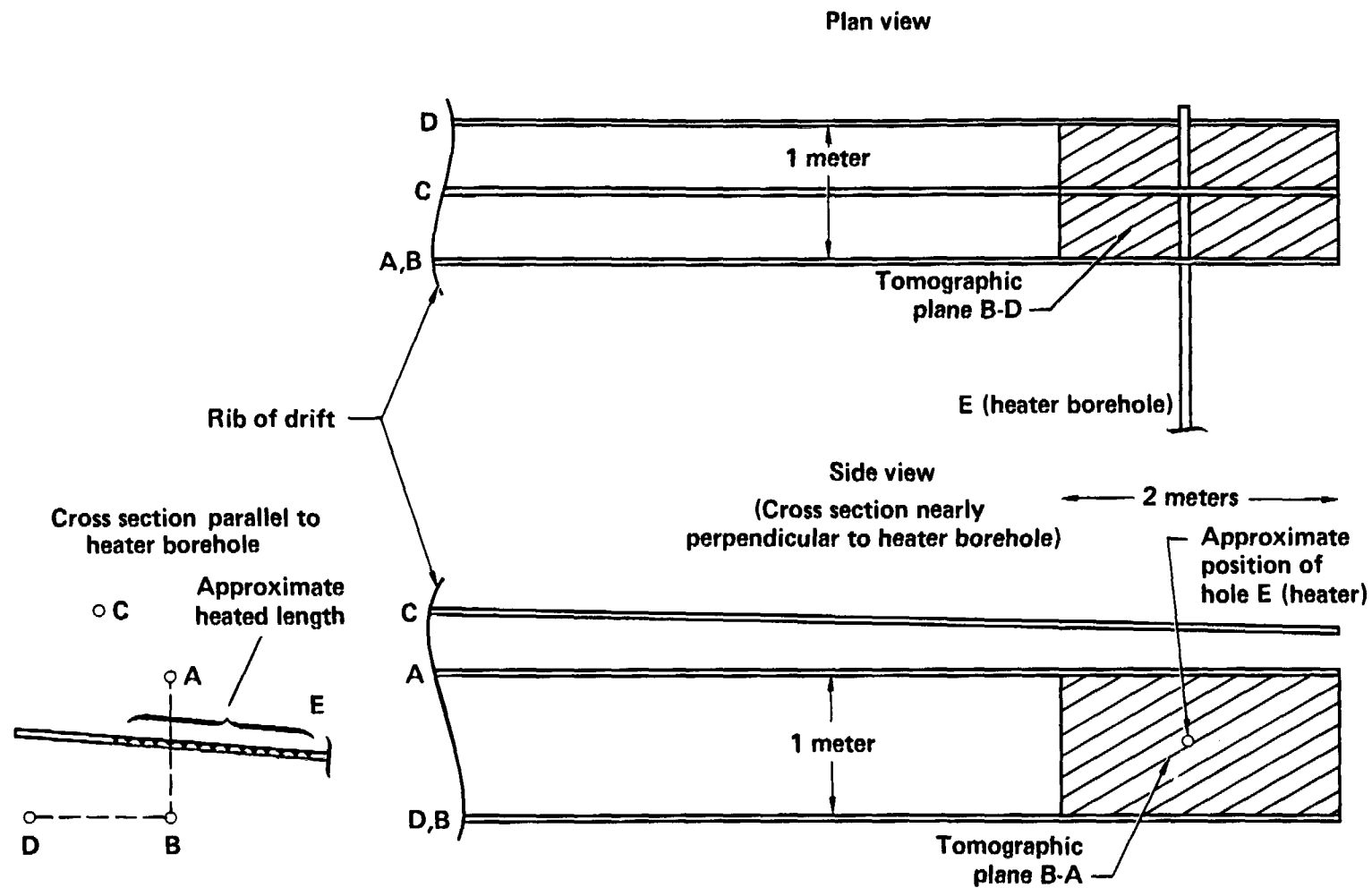


Figure 2. Borehole layout and measurement planes relative to the location of the heater borehole. Vertical and horizontal tomographic planes were sampled.

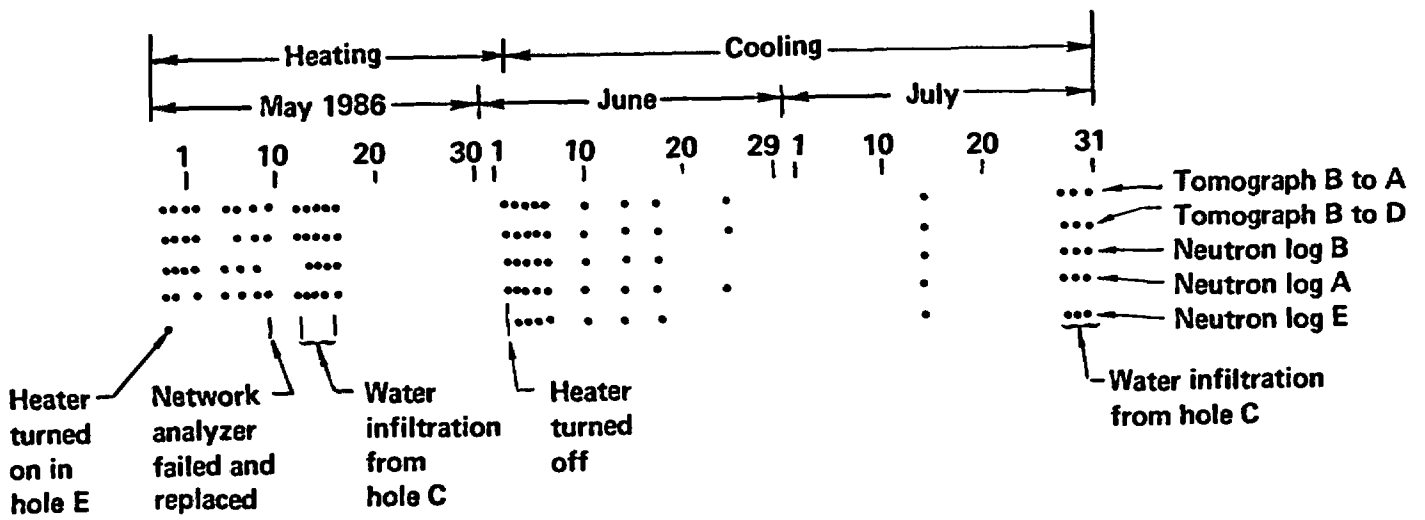


Figure 3. Experiment schedule followed during the heating and cooling phases of the experiment.

rock mass was allowed to cool. Water infiltration was also performed during the cooling phase.

Temperature logs of boreholes A, B and D were attempted but due to bad thermocouple connections, discovered late in the experiment, this data set was unusable. Unfortunately, the best temperature information we have is simply that during some of the heating phase, the EM antennas were too hot to handle when removed from the boreholes. After sufficient cooling, boreholes A, B, D and E were logged with a borescope to locate fractures and map their orientation. Core from these holes was also examined to locate fractures and other structures which may have played a role in local hydrology during the test.

Tomographs of electromagnetic permittivity at 200 MHz were made in two planes each 1 meter by 2 meters in the tuff heated by a 1 kilowatt heater. Tomograph data were taken over a period of three months during both heating and cooling of the rock mass. These tomographs required 44,982 individual measurements which were reconstructed into a total of 10,710 pixel elements of the 51 tomographs eventually used in the analysis. The volume of information resulting from the experiment complicated the process of analysis, therefore a video tape was used to aid in data interpretation. The tomographs were arranged chronologically, linear interpolation performed to fill in the gaps during periods when no measurements were made, and a video tape made of the tomographs compressing the experiment time scale from three months to 53 seconds. This format was useful in relating the temporal and spatial properties of the rock mass over a long time period. (It is unfortunate that this format does not lend itself to the written page.)

The experiment required integrated operation of several complex electronics instruments over a long period of time, and in an environment for which they were not designed. Line voltage surges, extreme dust and mechanical shock from high explosive detonations in the tunnel, and 100 percent humidity were part of the environment for instrumentation designed to work in a laboratory setting. The instrumentation was selected based on performance from many previous field deployments. We consider the resulting performance highly successful. Only a single failure occurred in a key piece in the system; a network analyzer was replaced May 9th (See Fig. 3) but its replacement operated trouble-free the remaining 83 days of the experiment.

3. RESULTS AND DISCUSSION

The objective of this experiment was to evaluate alterant geophysical tomography as a candidate technique for monitoring moisture content changes in the near field environment of a thermally simulated nuclear waste container in densely welded tuff. Without doubt, the best evaluation would be detailed comparison of the results from the experiment with measurements made by a technique already proven to do the same job. Such a proven technique does not exist and of course, if it did there would be no need to evaluate geotomography for this application. Therefore, we are forced to evaluate alterant geophysical tomography by using the tomographic results, along with the other available geophysical and geological data to develop a scenario for the hydrologic phenomena in the heater near-field during the experiment. If this scenario is sensible and self consistent we will conclude that geotomography may be a useful technique for mapping changes in moisture near an in situ heater.

3.1. LABORATORY MEASUREMENTS

To aid in interpreting the geotomographs we performed a series of laboratory experiments to measure the electromagnetic properties of densely welded tuff from G-tunnel as a function of water content. A rock sample was machined to fit into a 1.43 cm-diameter electromagnetic coaxial transmission line (Freeman, et al.; 1979). The sample did not have a visible fracture. The complex electromagnetic permeability (μ) and permittivity (ϵ) were calculated from values of transmission and reflection coefficients of the assembly, measured using an automatic network analyzer. Only one sample was tested using this procedure. Figure 4 shows the real part of the relative permittivity ϵ_r/ϵ_0 for this rock as a function of water content from dry to full saturation of the connected porosity (13.8 vol%). These results show a nearly linear relation between the variables over the full change of water content. This strong relationship exists because ϵ_r/ϵ_0 for water is about 80 (at 20°C) while that of silicate matrix is about 4. Therefore the effective permittivity of the combination strongly depends on the water fraction. We rely heavily on this fact to interpret the tomographs; a decrease in measured permittivity will be inferred as a decrease in water content of the rock mass and vice-versa.

It is important to emphasize, however, that the results in Fig. 4 cannot be used to infer the rock mass water content directly. One reason is that the tomographic data were not taken with antennas and measurement system calibrated for measurement of absolute permittivity. Another reason is that the laboratory data were taken only at room temperature. Although we know

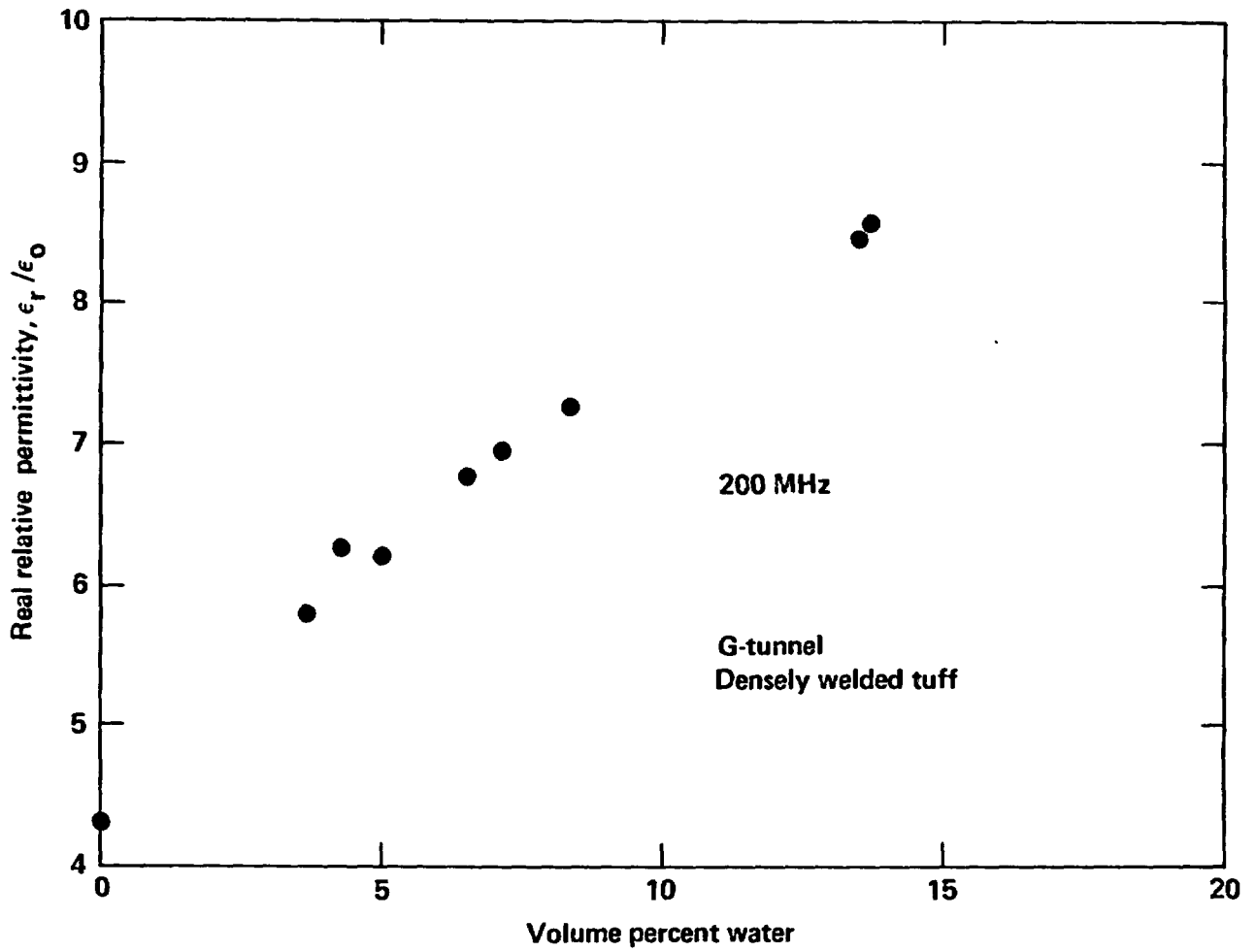


Figure 4. Laboratory measurements of the real part of the relative permittivity versus moisture content in a welded tuff sample at 20C.

experimentally that for the silicate matrix ϵ_r does not vary significantly with temperature (below 100°C), we know that the permittivity of water decreases with temperature. At 100°C ϵ_r/ϵ_0 for water is about 48 (Eisenberg and Kauzmann, 1969). The mixing rule of Meador and Cox (1975) relates ϵ_r of the rock mass, ϵ_k permittivity of the silicate matrix, ϵ_w permittivity of the pore water and ϵ_a permittivity of the pore air as follows:

$$\epsilon_r^x = (1 - \phi) \epsilon_k^x + S_w \phi \epsilon_w^x + (1 - S_w) \phi \epsilon_a^x$$

where ϕ is the porosity and S_w is water saturation. Hearst and Nelson (1985) indicate that in this equation the parameter x is about 0.5. Then for initial conditions $\phi = 0.15$ and $S_w = 0.85$ (about 20 C) where $\epsilon_k/\epsilon_0 = 5$, $\epsilon_w/\epsilon_0 = 81$ and $\epsilon_a/\epsilon_0 = 1.0$ we get $(\epsilon_r/\epsilon_0)^{1/2} = 3.1$. If all the pore water is heated to boiling but remains in the liquid state, we find $(\epsilon_r/\epsilon_0)^{1/2} = 2.8$. Heating the rock mass (without vaporizing the water) will result in only about a 10% change in $(\epsilon_r/\epsilon_0)^{1/2}$. It will be shown later that near the heater the measured permittivity $(\epsilon_r/\epsilon_0)^{1/2}$ changes by about 50% during the experiment. Therefore, even as the rock mass is heated, there will be a strong and direct relation between water content and $(\epsilon_r/\epsilon_0)^{1/2}$ measured in the tomograph so that qualitative interpretation of the images in terms of water content changes will remain reasonably valid even in the heated rock mass. The vapor phase of water should be essentially undetectable by electromagnetic tomography (Jordan, 1985) because in the vapor state the density of water molecules is so small.

3.2. ROCK MASS HEATING

A tomograph of measurement plane A-B is shown in Fig. 5. The data for this image was taken before the heater was turned on so it represents the background conditions with which subsequent alterant tomographs are compared. It shows no obvious pattern of permittivity distribution related to the heater position or to the measurement plane location. The heterogeneity probably represents initial distribution of water content and lithology of the rock mass in the plane between the boreholes. It is interesting to note that the average $(\epsilon_r/\epsilon_0)^{1/2}$ measured for the ambient conditions is approximately 3.0. Although we are uncertain of the system calibration and therefore cannot rely on the accuracy of absolute measurements of relative permittivity, this value is close to the value that was calculated above using the mixing rule and laboratory measurements of saturation, porosity and moisture content.

Figures 6 and 7 show two alterant tomographs, chosen to span the entire heating phase of the experiment (2.5 days and 34 days respectively). These data show an overall decrease of permittivity in both planes during heating. This is reasonable since we might expect a general drying throughout the region as the thermal field expands. In fact this permittivity decrease is monotonic during heating throughout the A-B image plane except during times when water was being added to the rock mass through borehole C. The drying appeared to be less intense in plane B-D than plane A-B and this is reasonable since the former was further removed from the heater. The changes in $(\epsilon_r/\epsilon_0)^{1/2}$ shown in Fig. 6 are larger than ± 0.04 which is the variation introduced by measurement imprecision.

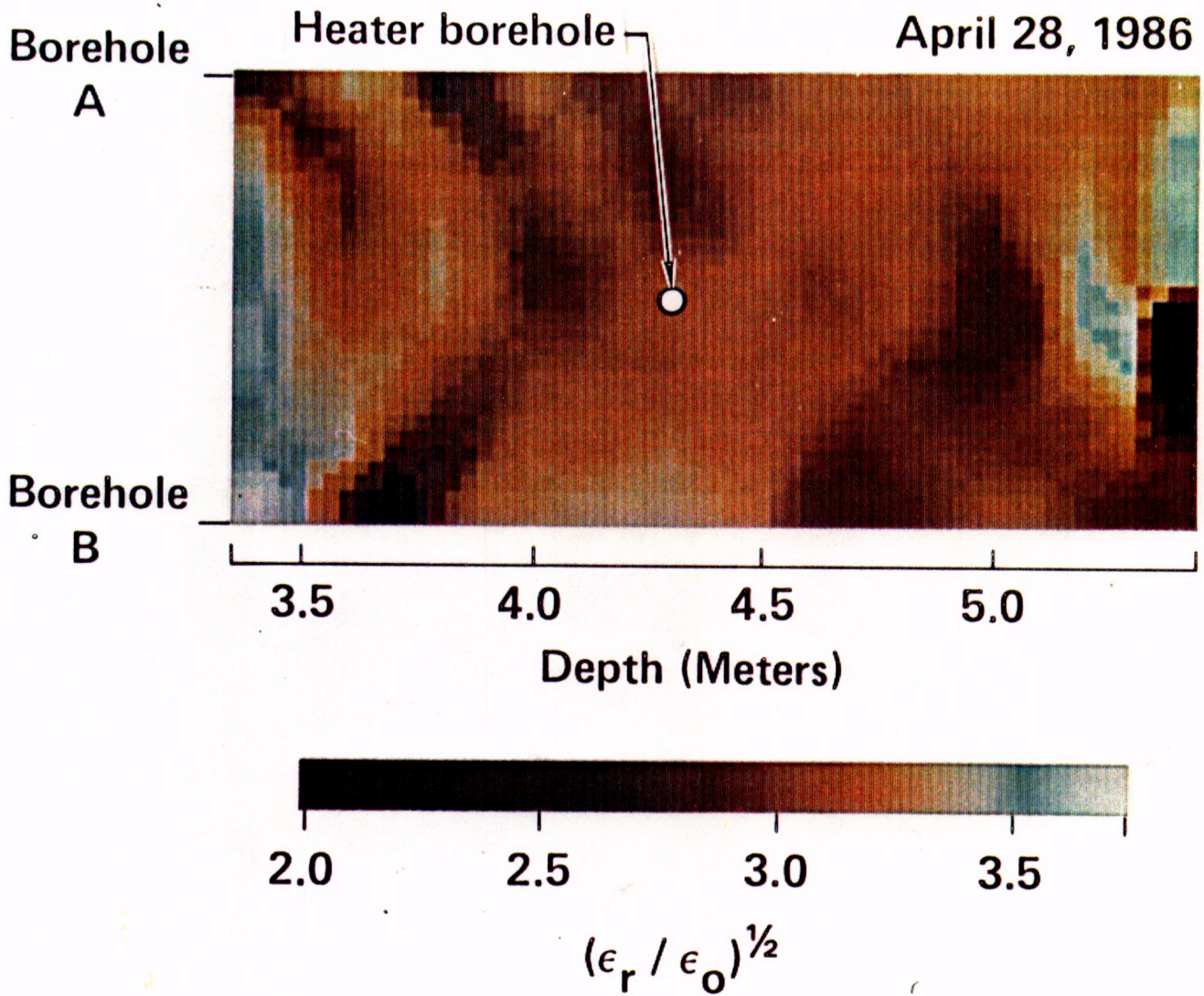


Figure 5. Baseline tomograph of the vertical measurement plane (defined by boreholes A and B) before the heater was turned on. The square root of the real part of the relative permittivity $(\epsilon_r / \epsilon_0)^{1/2}$ is represented by the gray scale shown at the bottom.

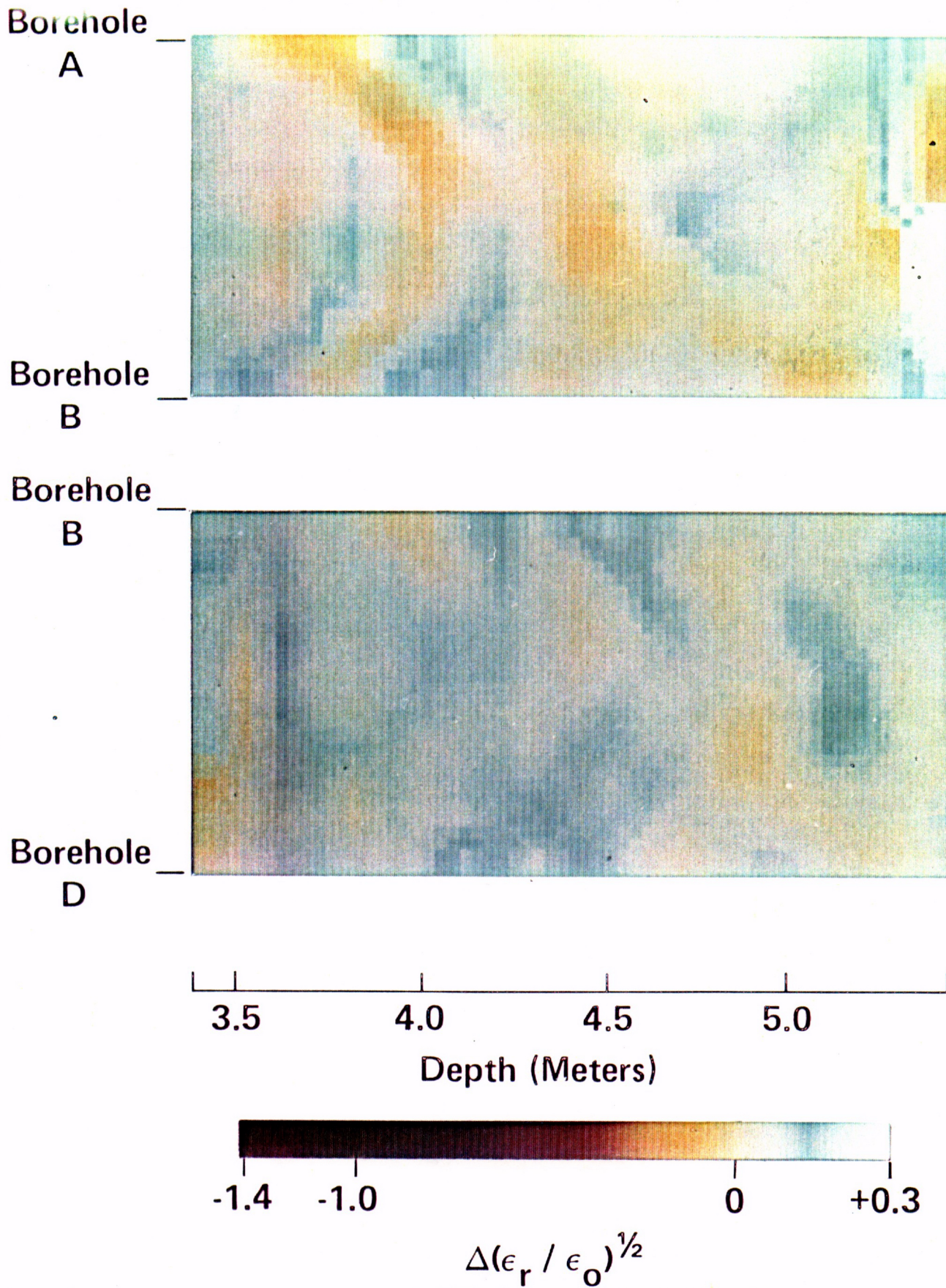


Figure 6. Alterant tomographs showing the changes in the square root of the relative permittivity $\Delta(\epsilon_r / \epsilon_0)^{1/2}$ after 2.5 days of heating. The top and bottom images represent the vertical and horizontal measurement planes, respectively. Negative changes in $\epsilon_r^{1/2}$ should indicate regions with decreasing moisture.

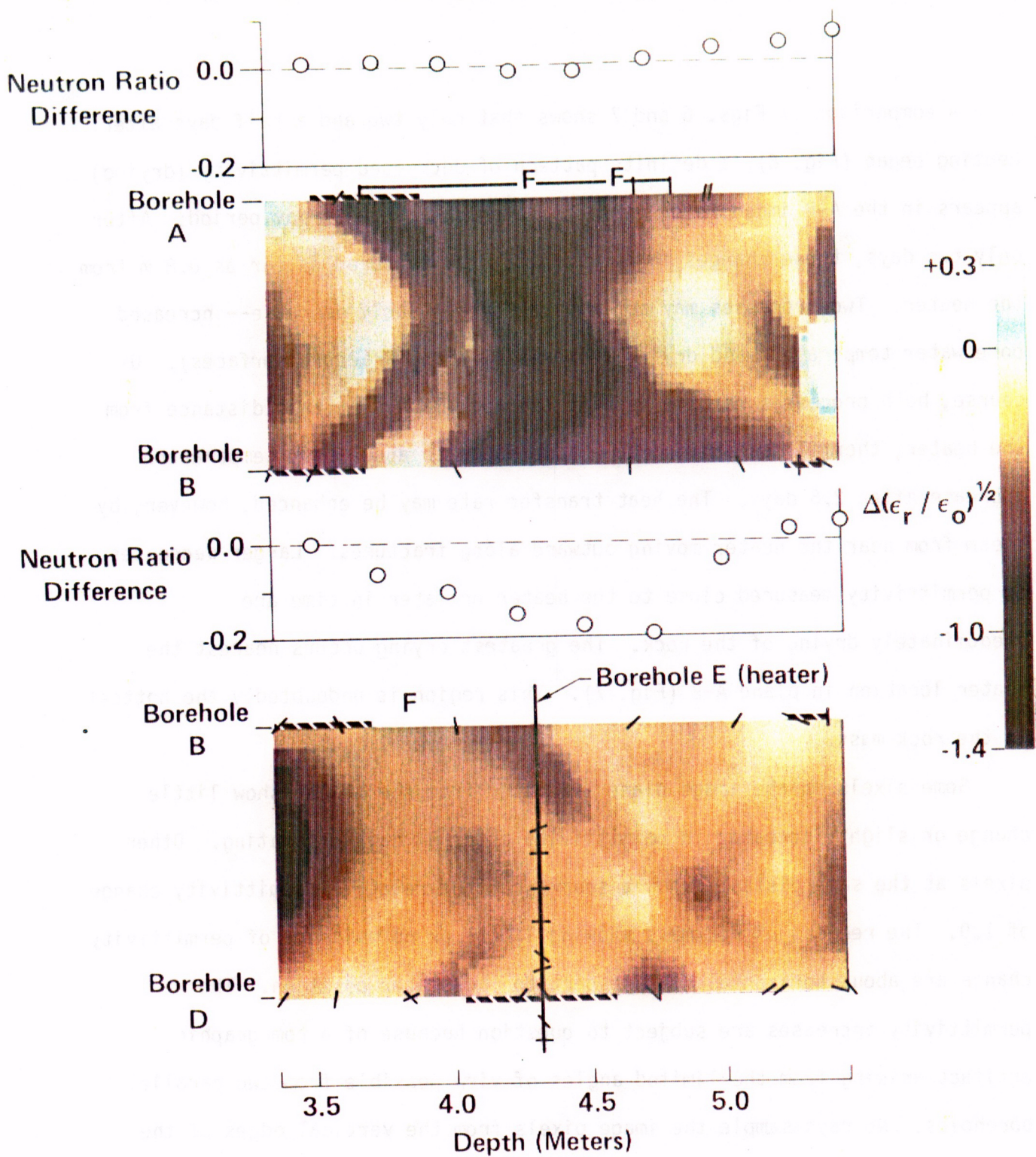


Figure 7.

Alterant tomographs of the changes in the square root of the relative permittivity $\Delta(\epsilon_r/\epsilon_0)^{1/2}$ after 34 days of heating. Both images use the color scale shown. Negative values of $\Delta(\epsilon_r/\epsilon_0)^{1/2}$ represent decreases in permittivity (dehydration) over the heating period. Fractures, as mapped along each borehole, are shown with the apparent dip (top panel) or strike (bottom panel) when orientation could be determined. When orientation could not be determined the letter F indicates a fracture location. A bracket is used along borehole A to denote a fracture roughly parallel to the hole axis. The symbol --- denotes multiple fractures or broken borehole wall. Borehole E, with fractures mapped along part of its length, is shown projected into the B-D plane. In the top panel, differences in neutron log ratios are plotted. The upper plot is for data from borehole A and the lower plot is for borehole B. Negative differences indicate a dehydration of the rock mass.

A comparison of Figs. 6 and 7 shows that only two and a half days after heating began (Fig. 6), a definite pattern of decreased permittivity (drying) appears in the A-B image which persists, throughout the 34 day period. After only two days, these changes in permittivity are measured as far as 0.8 m from the heater. Two processes may contribute to this early decrease--increased pore water temperature and drying (especially along fracture surfaces). Of course, both processes require heating the rock mass. At this distance from the heater, thermal conduction could contribute to about 10°C temperature increase after 2.5 days. The heat transfer rate may be enhanced, however, by steam from near the heater moving outward along fractures. Larger decreases in permittivity measured close to the heater or later in time are predominately drying of the rock. The greatest drying occurs nearest the heater location in plane A-B (Fig. 7). This region is undoubtedly the hottest in the rock mass.

Some pixels on the image plane 1/2 meter from the heater show little change or slight increases in permittivity after 34 days of heating. Other pixels at the same distance show a square root of relative permittivity change of 1.0. The regions of rockmass showing little or no evidence of permittivity change are about horizontal with respect to the heater position. The permittivity increases are subject to question because of a tomographic artifact arising from the limited angles of view possible from two parallel boreholes. No rays sample the image pixels from the vertical edges of the image space. Therefore the sum of pixel values in each horizontal row must remain unchanged from that of the initial guess image. Because of this, a decrease in permittivity corresponding to the rock near the heater must be

compensated by corresponding changes in the opposite sense by other pixels in the row for the sum to be invariant. In other words, the image cannot show a localized anomaly without some horizontal distortion. We will refer to this as limited view distortion (Burkhard, 1980). This distortion is not a problem when the region is sampled from all sides. In the alternating tomographs of Fig. 7, the permittivity decrease surrounding the heater is flanked on both sides by permittivity increases. It is not known to what extent this limited view distortion affects the image fidelity but it is certainly a factor which must be considered when interpreting the images.

Drying is not restricted to the immediate vicinity of the heater -- it is also not radially symmetric about the heater. The distribution of dehydration is apparently controlled by strong heterogeneity in the rock mass. Dominant is a dehydrating zone, roughly vertical, about 1/2 meter wide and centered on the heater. The vertical nature of this anomaly may be somewhat exaggerated by the limited view distortion discussed above. The anomaly may also be distorted because of contrast in permittivity between dry rock near the heater and the wetter rock around it. This is evident since the anomaly extends to the tomograph edge B in plane A-B. What appears to be the image of the same fracture in B-D is much less prominent in that plane and probably less distorted. However, this distortion from permittivity contrasts cannot be too extreme because the same pattern that appears only two days after heating starts, persists largely unchanged, throughout the 34 day heating period. Initially the permittivity contrasts were too small to cause such distortions. Therefore we conclude that dehydration is not symmetric about the heater location. A likely explanation for the dry region near the heater

is the vertical orientation of most fractures in the formation (Langkopf and Eshom, 1982; Winograd and Thordarson, 1975). The image may reflect dehydration of a rock volume bounded by nearly vertical fractures. The vertical nature of this anomaly may be exaggerated. Additional dehydration probably occurred along the boreholes, especially A and B, since they are excellent conduits for steam away from the heated rock mass.

Some anomalies in the tomographs of Figs. 6 and 7 are linear in shape, suggestive of fracture influence during dehydration. Some of these same lineations were present before heating (Fig. 5) suggesting initially enhanced moisture content in fractures. Superimposed on the tomographs of Fig. 7 are actual fracture locations and orientations as mapped using a borescope in boreholes A, B and D. Several anomalies at the A-B tomograph edge correspond approximately with both fracture location and orientation. This correlation appears more than fortuitous and suggests that fractures play an important role in dehydration of the rock mass. One possible interpretation is that as the thermal field expands, dehydration is most rapid along fractures. Water vapor leaves the matrix by preferentially moving towards the fracture where it then moves along the fracture toward a cooler part of the rock mass. This dry region around the fractures expands with time. This phenomenon has previously been observed in laboratory studies of welded tuff (Daily, et al., 1986). A few of the fracture orientations in Fig. 7 differ from the anomaly orientations at the image edge. This may result from the convoluted nature of the fractures (Langkopf and Eshom, 1982) or the limited image resolution near the edges (Ramirez, 1986).

It should be noted that if rockmass porosity averaged over some pixel elements is much larger than that for other pixels, permittivity changes in the alterant tomographs must be interpreted with care. From equation (1), we find that the difference in measured square root of permittivity is related to a change in saturation by

$$\Delta(\epsilon_r^{1/2}) = \phi (\epsilon_w^{1/2} - \epsilon_a^{1/2}) (\Delta S_w)$$

The measured permittivity change is proportional to the product of porosity and water saturation change $\phi (\Delta S_w)$. If ϕ is very large for a portion of the rock represented by a particular pixel -- say from multiple fractures such as might be present along a shear zone -- a modest change in saturation can result in a substantial change in permittivity. In other words the correct interpretation of a permittivity change is a change in water volume fraction. In fact this may explain the correspondence between tomograph anomalies before heating (Fig. 5) and alterant tomographs during heating (Fig. 6, top panel). If the enhanced permittivity regions in Fig. 5 represent fracture water (large average values of ϕS_w for those image pixels) then very slight drying early in heating may have resulted in large permittivity changes in those regions in Fig. 6 (large average values of $\phi (\Delta S_w)$ for those image pixels). Saturation changes (ΔS_w) in the matrix could have been comparable but because the average porosity for those pixels may be much smaller, the product $\phi (\Delta S_w)$ and therefore $\Delta \epsilon_r^{1/2}$ in the alterant tomograph would be proportionally smaller.

Figures 6 and 7 show many of these low water content anomalies as linear features nearly radial to the heater location. This tendency for radial

orientation is not understood and may be an image distortion. The limited view distortion discussed above may suppress features to either side of the heater, leaving an apparent radial orientation for the remaining anomalies. We do also expect some distortions or artifacts in the images since straight ray paths are assumed in the image reconstruction algorithm. This assumption is only approximately valid when changes in permittivity in the plane of measurement are small enough. Such distortions are most likely to occur when there are large contrasts of wave velocity in the image plane such as we have during the latter stages of drying. On the other hand there are valid reasons for accepting as real the tendency of radial drying features. First, the shape and location of the features remain unchanged from the earliest alterant tomographs when the wave velocity contrasts were quite small (i.e., image distortion was minimal). Second, for the most part, the features match the location and orientation of fractures mapped at the boreholes.

Tomographs of plane A-B clearly show strong drying of the rock mass near the heater. Total drying of a rock volume 1.6 m long (the heater length) and 0.25 m in radius (assuming 14% porosity and 90% saturation) results in 0.04 m^3 or 40 liters of water. If most of this water stayed within the rock mass (not exiting the measurement boreholes), it would eventually return to liquid when it reached rock that cooled it below the dew point. This significant amount of water should be observed if it condenses within or if it moves through one of the tomographic planes. Note however, that there is no indication of permittivity increase in plane B-D during heating. This is evidence that water, which certainly must have been produced from the drying rock near the heater may not have moved as liquid by gravity along fractures through plane

B-D and away from the experimental area. Possibly the water moved as steam up through the fracture system and condensed in the cooler rock mass above the experiment area. This hypothesis is supported by the neutron log data shown in Fig. 7. Along borehole B, below the heater, the data show a strong decrease in count rate implying a dehydrated zone centered roughly at the location of the heater. However, along borehole A, above the heater, the data show an overall increase in water content of the rock mass.

A comparison of the neutron logs and the images shows some agreement between the two along borehole B and no agreement along borehole A. The neutron log and the tomographic image are sensitive to different volumes of the rock mass. The tomographs only map water content changes in a thin plane between the boreholes. The neutron tool senses water content changes in a volume of radius ~ 25 cm around the borehole. Perhaps the lack of correlation between the borehole A neutron log and the tomograph along borehole A results from the neutron log sensing simultaneously dehydration below the borehole and hydration above the borehole. On the other hand, along borehole B the neutron log probably sampled only dehydrated rock and, in this case, there is a qualitative correlation between the image and the neutron measurements.

3.3. ROCK MASS COOLING

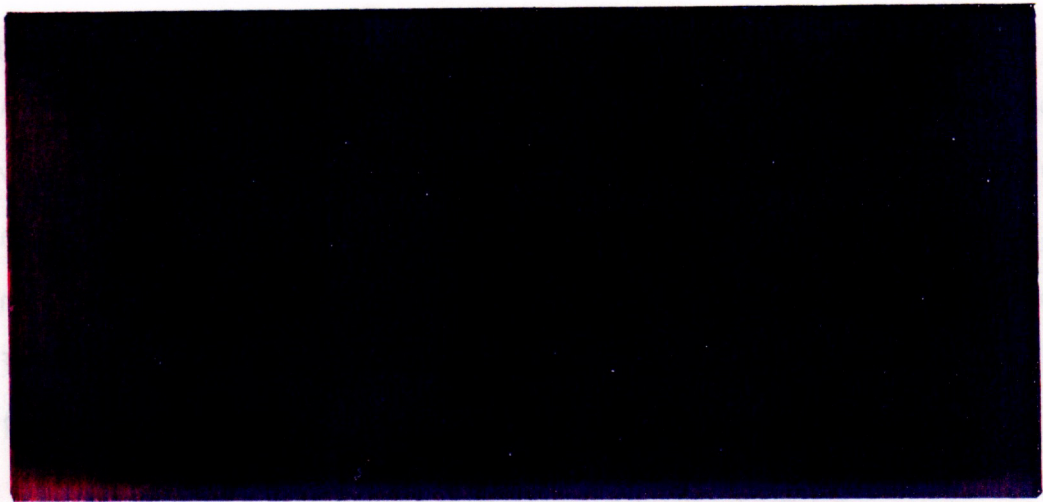
Figures 8 and 9 show alterant tomographs chosen to span the cooling phase of the experiment. In plane A-B there is an overall increase in permittivity during the period, implying a general rehydration of the rock mass. This is reasonable since we expect a gradual rehydration as the thermal field collapses, steam condenses and water can re-enter the rock mass. There is

Borehole A

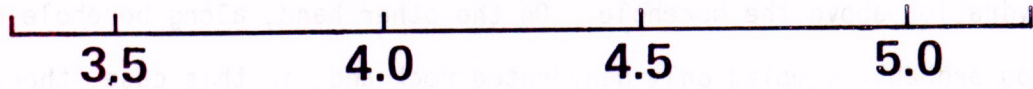


Borehole B

Borehole B



Borehole D



Depth (Meters)



$\Delta(\epsilon_r / \epsilon_0)^{1/2}$

Figure 8. Alterant tomographs of changes in the square root of the relative permittivity $\Delta(\epsilon_r / \epsilon_0)^{1/2}$ in both vertical and horizontal measurement planes approximately 4 days after the heater was turned off. These changes are relative to the last day of heating. Positive values of $\Delta(\epsilon_r / \epsilon_0)^{1/2}$ indicate increases in permittivity and water content over the period.

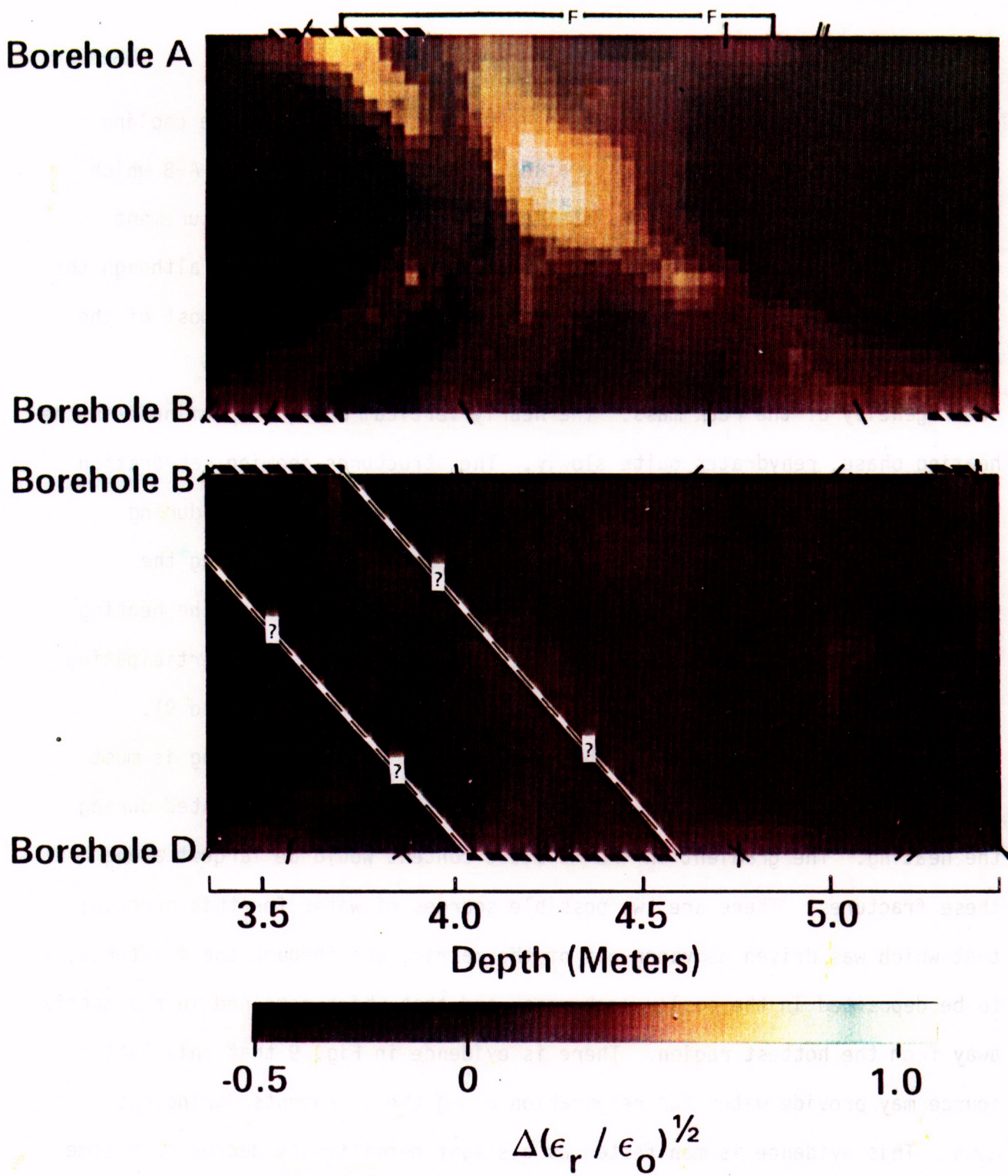


Figure 9. Alterant tomographs of changes in the square root of the permittivity $\Delta(\epsilon_r / \epsilon_0)^{1/2}$ in the vertical and horizontal measurement planes 56 days after the heater was turned off. Positive values of $\Delta \epsilon_r^{1/2}$ indicate increases in permittivity (and water content) over the period. The symbols for fractures along each borehole are described in Fig. 7.

C-05

indication of only slight rehydration in plane B-D. Early in the cooling phase, a definite pattern of rehydration is established in plane A-B which becomes more pronounced but persists in shape throughout the measurement period. Again, this pattern is not symmetric around the heater, although the largest increase in water content occurs near the heater. Over most of the image plane A-B the moisture increase is apparently controlled by heterogeneity of the rock mass. The nearly vertical zone, so prominent in the heating phase, rehydrates quite slowly. The structures showing rehydration in Fig. 9 are even more linear in nature than those which dehydrate during heating. Again, the images are suggestive of fractures dominating the hydrology. In fact, there is a good enough correlation between the heating and cooling tomographs to argue that the same fractures may be participating in both drying and rewetting of the rock mass (compare Figs. 7 and 9).

We suggest that as the thermal field collapses, rewetting is most rapid in the matrix along those fractures which were most dehydrated during the heating. The gradient in the moisture content would be largest along these fractures. There are two possible sources of water for this process; that which was driven as vapor out of the matrix, and through the fractures, to be deposited in the cooler rock mass, and that which remained in the matrix away from the hottest region. There is evidence in Fig. 9 that this latter source may provide water for rehydration along the lineaments during cool down. This evidence is manifested as a slight permittivity decrease in some regions adjacent to the rehydration features, and is most evident in the cool down tomograph of Fig. 9. These regions may be artifacts from limited view distortion. However, if the residual matrix water entered the dry rock

adjacent to fractures, it did so by moving through capillary paths driven by the gradient in matrix potential. The tomographs show no evidence for either a sharp or a diffuse boundary during the first two months of cool down which might be construed as a single wetting front. In the conceptual models for waste package it may be inappropriate to talk about rehydration in terms of such a boundary.

The neutron log data acquired during cool down (Fig. 10) are consistent with the interpretation of the tomographs. They show an overall increase in water content below the heater and a decrease in water content above the heater. However, saturation levels measured with the neutron probe (as well as water content levels inferred from the tomographs) did not return to the pre-experiment, background levels during the two month cool down period.

3.4. WATER INFILTRATION

For brief periods during both the heating and cooling phase of the experiment, distilled water was added to the rock mass (see Fig. 3) via borehole C (Fig. 2). The purpose of this procedure was to determine if large quantities of liquid water could be imaged by geotomography as it perturbed the system. Figure 11 is an alterant tomograph comparing images taken just prior to and during water infiltration with the heater on. In plane A-B, while there is still strong dehydration taking place in some regions, there is also clear evidence of isolated permittivity increases. Apparently, the water enters plane A-B via part of the fracture parallel to the axis of hole A at the top of the image and exits at borehole B via the fracture near 4.7 m and the highly fractured region near 3.7 m. Before water infiltration began, a

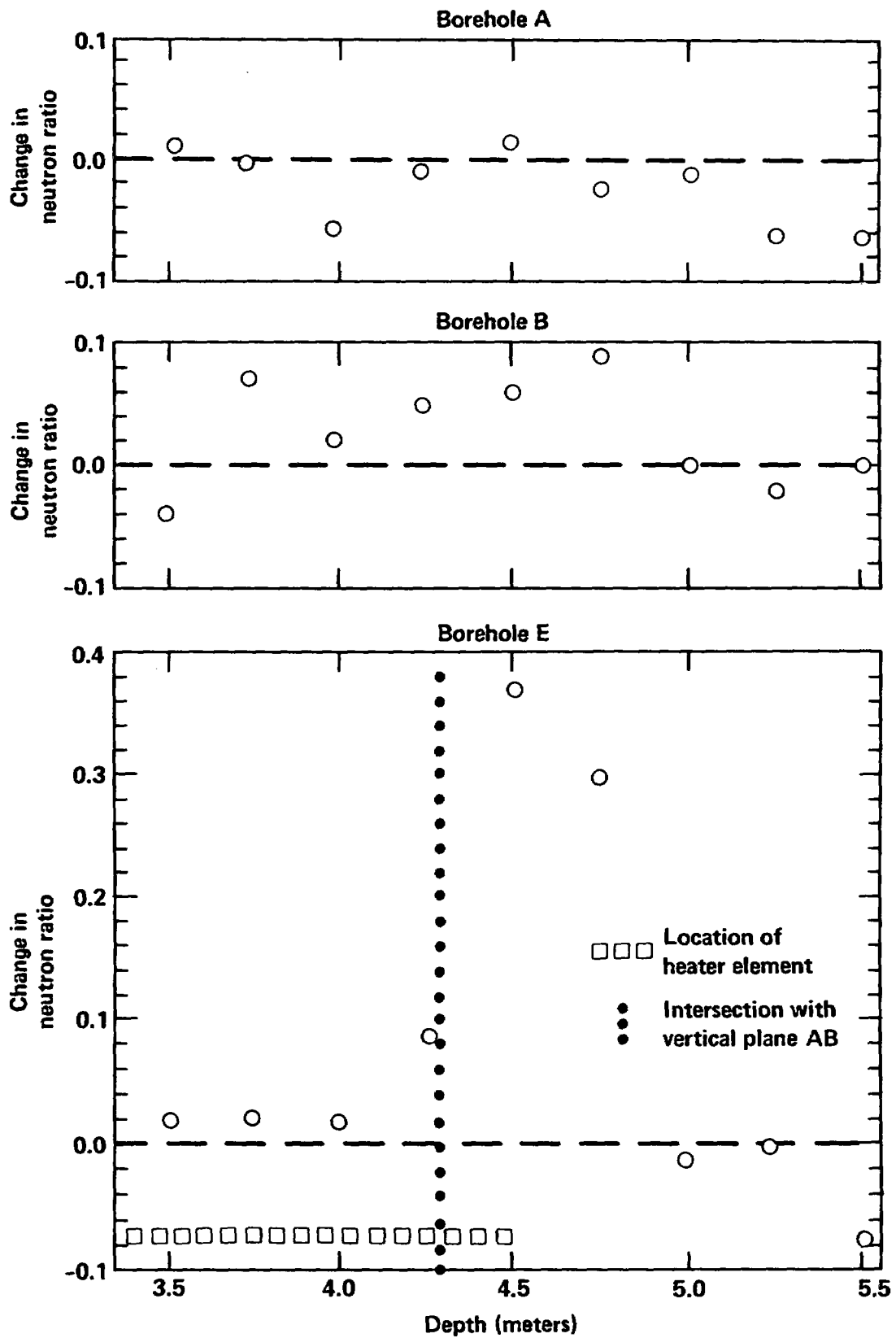


Figure 10. Changes in neutron ratios (counts/calibration) along boreholes A, B, and E over the 56 day cooling period. Positive changes indicate water content increase relative to the last day of heating.

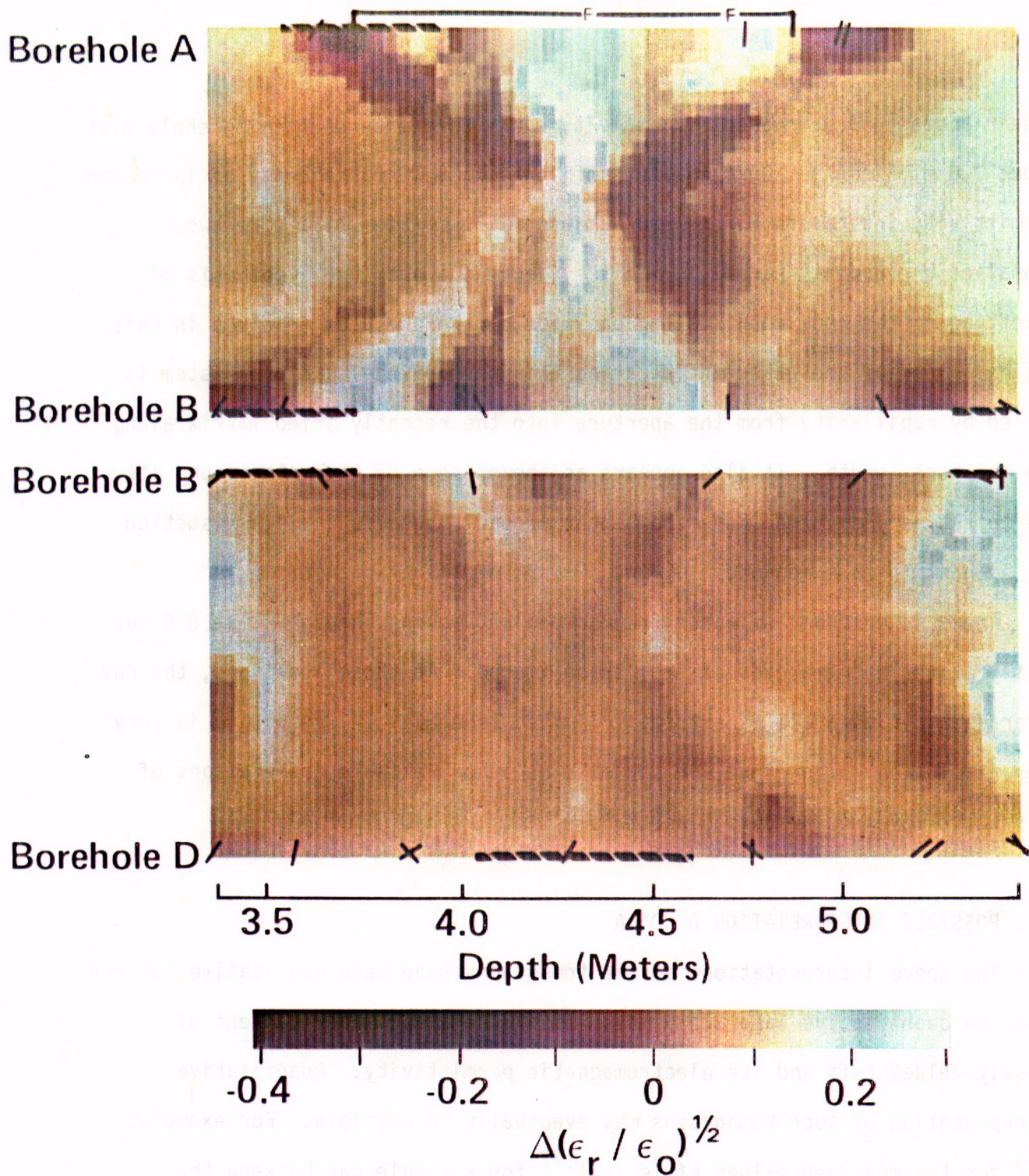


Figure 11. Alterant tomographs of the square root of the relative permittivity $\Delta (\epsilon_r / \epsilon_0)^{1/2}$ in the vertical and horizontal measurement planes after infiltration of distilled water (see Fig. 3) from borehole C. Positive values of $\epsilon_r^{1/2}$ indicate increases in permittivity (and water content). Symbols used to denote fractures along boreholes are described in Fig. 7.

linear anomaly of decreased permittivity was imaged intersecting borehole B at about 3.6 m (Fig. 7). During water infiltration a linear anomaly of increased permittivity intersects borehole B at about 3.75 m (Fig. 11). The two anomalies are roughly parallel. This evidence supports the hypothesis of rewetting in the rock matrix along one side of the presumed fracture in this region. Perhaps the water infiltrating this part of the fracture system is pulled by capillarity from the aperture into the recently dried matrix along the fracture length. It also appears as though some of the water found its way to the very dry zone near the heater probably because capillary suction was highest in this region.

There is evidence of water from borehole C moving through plane B-D but mostly at the extreme ends of the region imaged. At these locations, the ray coverage and view angle is extremely limited (see Fig. 1A) resulting in very poor resolution. Therefore, we can make no other reliable observations of this water movement through plane B-D.

3.5. POSSIBLE INTERPRETATION OF DATA

The above interpretations of the tomographs have been qualitative but are based on quantitative laboratory measurements relating water content of densely welded tuff and its electromagnetic permittivity. Quantitative interpretation of such tomographs may eventually be possible. For example, consider the measured values of $(\epsilon_r/\epsilon_0)^{1/2}$ for a single ray between the 4.3 meter depth locations in boreholes B and A (this ray passes within 10 cm of the heater). Each permittivity value measured along this ray during the experiment was converted to a water content for the rock by simply using

Fig. 4. No correction was made for temperature dependence of water permittivity on the field measurement system calibration and values outside the range plotted in Fig. 4 were obtained by linear extrapolation. The resulting average water content of the rock along this ray is plotted as a function of time in Fig. 12.

Figure 12 is consistent with the qualitative interpretations already drawn from the tomographs. Near the heater, drying proceeded rapidly and resulted in substantial changes in moisture content. During cool-down, drying was much more gradual and involved comparatively small changes in moisture content. Small increases in moisture content are even recorded when water was added to the rock mass through borehole C during heating and cooling. However, the important point of this figure is that quantitative interpretations of the data may be possible. The initial water content of 17% is certainly reasonable for this formation (Wolfsberg, 1980; Zimmerman and Blanford, 1986). The driest value of -2.4 vol. % is obviously unphysical. However, the analysis is quite simplistic (e.g., it ignores the temperature dependence of ϵ_r for water) and the experiment was not designed to yield quantitative results (e.g., system calibration was not sufficiently accurate). Our assumption of the initial water content in the rock along this ray may be incorrect. Correction of any deficiency could shift the data a few percentage points. We are encouraged that such EM data can probably be interpreted quantitatively to map moisture content in the rock mass with straightforward extensions of our analysis and experimental technique.

A hydrologic scenario can be postulated based on the experiment results which we have discussed. When the heater in the rock was turned on a thermal

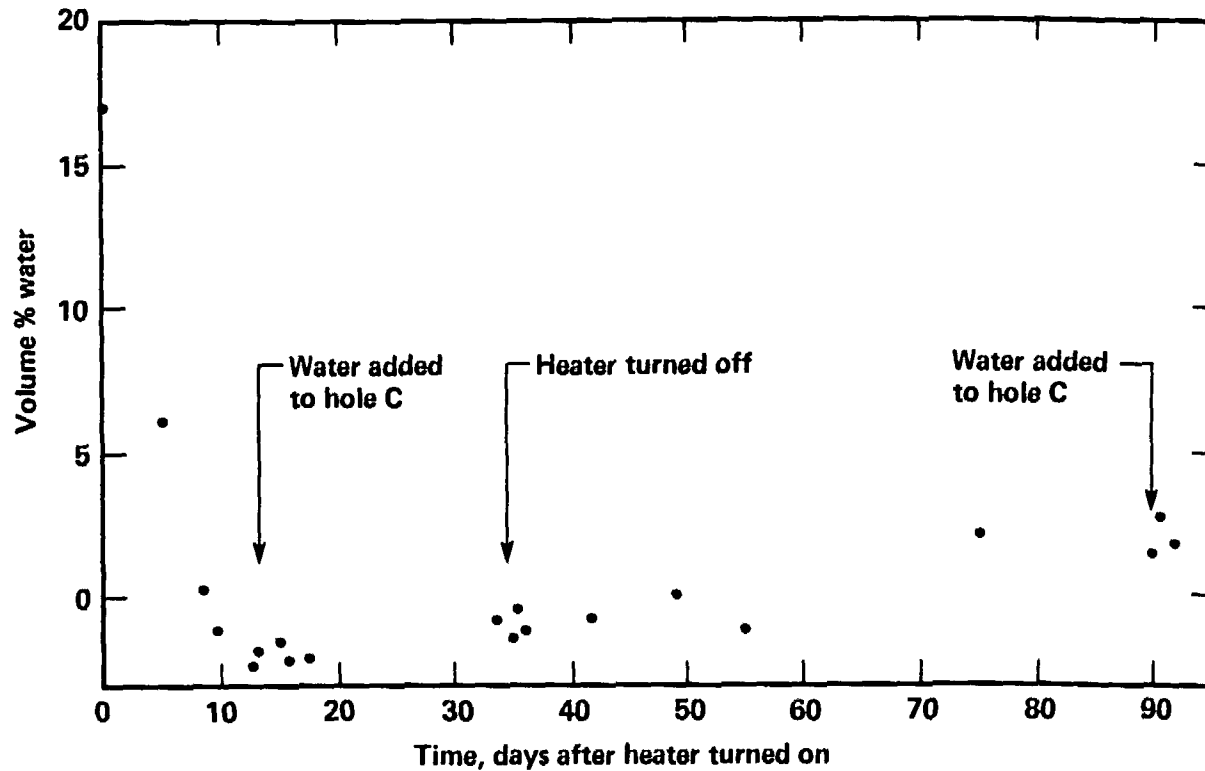


Figure 12. Water content averaged along the ray at 4.3 meters depth between boreholes B and A as a function of time. Each point was obtained by converting the in situ value of $(\epsilon_r/\epsilon_0)^{1/2}$ measured along the ray to a volume % water content using laboratory data (or extrapolation) from Fig. 4.

front expanded into the rock mass. As the temperature in a given pore space increased, the vapor pressure increased and the thermal gradient imposed by the heater was translated into a vapor pressure gradient. Water vapor moved, as a result of this gradient, through the matrix to the nearest pressure sink -- any fracture or boreholes hydrologically connected to the large low pressure reservoir of the surrounding rock mass environment. The resulting steam migrated upward through the fracture network until it reached rock which cooled it below the dew point. There, it condensed on the fracture wall. Apparently the fracture system was capable of holding most of this water by capillarity so that very little ran down the fractures by gravity or else the condensate was drawn by capillarity into the matrix. This process of drying occurred initially adjacent to the heater which is also the location of largest water content loss. The next most pronounced drying occurred more distant from the heater along fractures. In general, rock matrix furthest from fracture surfaces did not efficiently dry within the time scale of our experiment. It is clear that fractures played an important role in drying of the rock mass.

When the heater was turned off and the thermal front collapsed, some of the rock mass that dehydrated during heating began to rewet. However, the rewetting process was not simply the reverse of drying. As the temperature decreased in a given pore space the vapor pressure dropped. A capillary gradient formed between pores depleted of water and pores further from the heater containing more water. This gradient forced water to move from the wetter towards the drier pores. This capillary rehydration was most pronounced where drying was most severe and the moisture gradients highest --

adjacent to the heater. This very near field volume rewetted first and achieved the largest water content change. Further from the heater, where drying was predominately along fractures, the same phenomenon occurred. The driest regions adjacent to the fracture aperture rewet at the expense of moisture content of the rock further into the matrix.

4. SUMMARY AND CONCLUSIONS

This report describes an experiment which evaluated the effectiveness of alterant geophysical tomography in mapping changes of in situ moisture content in a thermally disturbed welded tuff rock mass. The experiment was conducted in Tunnel Complex 6 at the Nevada Test Site, Nye County, Nevada. Tomographs of electromagnetic permittivity at 200 MHz represented two planes in the rock, each one meter by two meters. Measurements were made over a three month period as the rock was heated by a 1 kilowatt heater and as the rock cooled. A total of 44,982 electromagnetic measurements were made and used to reconstruct 51 tomographs. The instrumentation required to make these measurements performed satisfactorily over a 3-month period in a relatively hostile underground environment.

The effectiveness of electromagnetic geophysical tomography to detect cross-hole changes in moisture content was evaluated by comparing the tomographs with other geological and geophysical data. Based on these comparisons, inferences are made on how moisture moved. We considered whether these inferences are sensible and self consistent, as a measure of evaluating if electromagnetic geophysical tomography may provide a viable way of monitoring in situ moisture content changes. This evaluation approach is by

necessity indirect because we know of no other proven techniques which could be directly compared to the electromagnetic tomographs.

The electromagnetic tomographs, the neutron logs and the fracture maps were used to infer water flow paths. Conclusions based on analysis of these data are as follows:

1. The changes in moisture content inferred from the tomographs generally agree with a priori expectations of the hydrologic response. As the rock temperatures increased the tomographs show that rock in the immediate vicinity of the heater loses moisture, and that this drying region grows larger with time. The greatest decrease in moisture content was observed around the heater.

2. Anomalies indicative of drying approximately coincided in location and orientation with fractures mapped along the borehole walls. One interpretation is a preferential drying along fractures which has been independently observed during laboratory experiments (Daily, et al., 1986).

3. After the heater was turned off and the rock cooled, the largest increases in moisture content occurred in the immediate vicinity of the heater. Also, anomalies indicative of rewetting coincide with fractures mapped in the boreholes. The tomographs suggest that fractures play an important role in how the rock dries and rewets.

4. The changes measured in $(\epsilon_r/\epsilon_0)^{1/2}$ were typically much larger than the variation which would be introduced by imprecision (± 0.04) associated with the measurement. This suggests that the observed anomalies are not artifacts of measurement noise. Although the experiment was not designed to yield quantitative values of moisture content in the rock mass, a simple analysis

was performed to make such estimates from the data. Considering the assumptions used, these estimates were fairly close to a priori knowledge, implying that in future experiments it may be possible to make reliable quantitative measurements of moisture content from electromagnetic tomographs.

From the results of this experiment we conclude that geophysical tomography can provide useful information on the hydrology near a heater in densely welded tuff. This conclusion is based on the fact that the experimental results were self consistent and in good agreement with a priori knowledge. We consider this conclusion preliminary, however, until the tomographic data can be analyzed using an inversion algorithm consistent with the large contrasts in measured signal velocity. This analysis is presently underway.

APPENDIX A

Description of Geotomography Algorithm

Computerized axial tomography (CAT) began a revolution in medical diagnostics because of its ability to display spatial distribution of x-ray attenuation for cross-sections of the body. Such tomographic or image reconstruction methods are applicable whenever line integrals of a parameter such as x-ray attenuation are available along many different orientations through a target. For the geophysical case, electromagnetic or acoustic energy is more appropriate for diagnostic probing, since the physical scale and scanning geometry are different from the medical case. Nevertheless, insofar as signal attenuation rate or propagation velocity characterizes the geology, geological characteristics can be imaged similar to the way medical tomographs are obtained. In the application considered here, the scanning paths are between boreholes in a fractured rock mass. A single transmitting antenna is placed in one borehole and a single receiving antenna is placed in the other. From a multitude of source receiver locations, a region between the holes is sampled along a large number of different paths of various orientations (Fig. A-1). The received signals carry the time-of-flight information for velocity measurements and amplitude information for attenuation measurements. Note, though, that the region is sampled from only two sides. This is in contrast to medical tomography where the target can be examined from all sides. This limited view angle for geotomography results in truncated projection and subsequent distortions in the image (e.g., Menke, 1984; Ramirez, 1986).

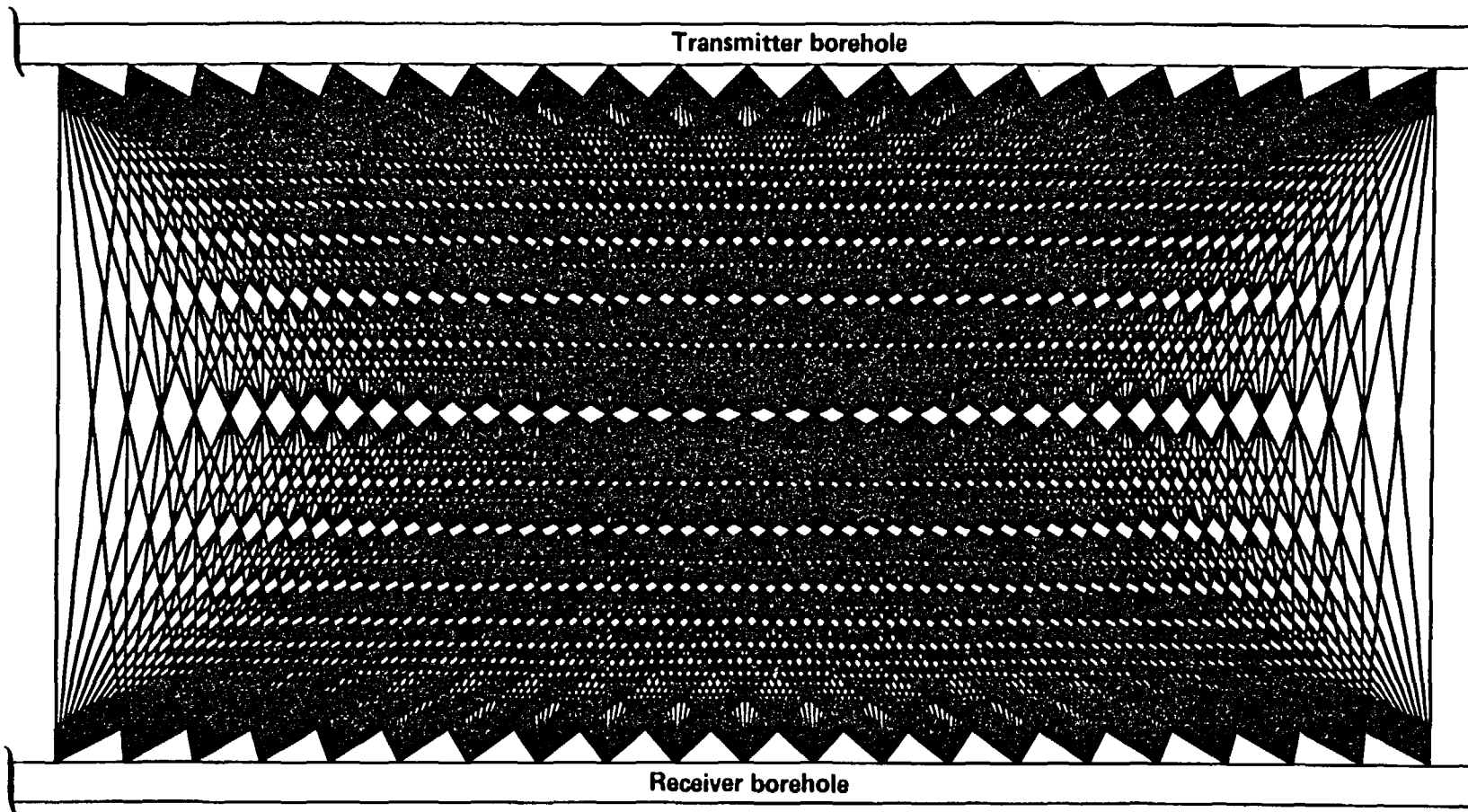


Figure A-1. Transmission paths between boreholes. A total of 441 ray paths were used to sample the rock mass between a single transmitting antenna in one borehole and a single receiving antenna in another.

The model we use for cross-borehole image reconstruction is shown in Fig. A-2. A typical ray path is indicated for electromagnetic signal propagation along a ray path approximated by a straight line. For the current application the ray paths are from 1.0 to 2.24 meters long and the source frequency is swept from 185 to 215 MHz.

The region in the plane between the boreholes is represented by some material parameter such as velocity $v(x,y)$ or attenuation rate $\alpha(x,y)$ which is to be calculated. Attenuation rate is a measure of how rapidly signal energy is dissipated with distance. However, work reported herein deals with signal phase velocity, therefore we illustrate the analysis by writing the relation between it and total signal delay along the k th path R_k

$$t_k = \int_{R_k} \frac{ds}{v(x,y)} \quad k = 1, 2, \dots, K \quad A-1$$

We want to reconstruct an image of the velocity function $v(x,y)$ from line integral data t_k collected from K rays of Eq. 1A. These are a set of K linear equations which can be solved for $1/v(x,y)$. Typically, Eq. 1A is converted to a discrete form by superimposing an $I \times J$ grid on the image plane (as in Fig. 2A) so that the discretized $1/v(x,y)$, which we denote $1/v_{ij}$, can be assumed constant over each cell. This approximation results in a system of K equations in $I \times J$ unknowns;

$$t_k = \sum_i^I \sum_j^J \Delta s_{ijk} / v_{ij} \quad k = 1, 2, \dots, K \quad A-2$$

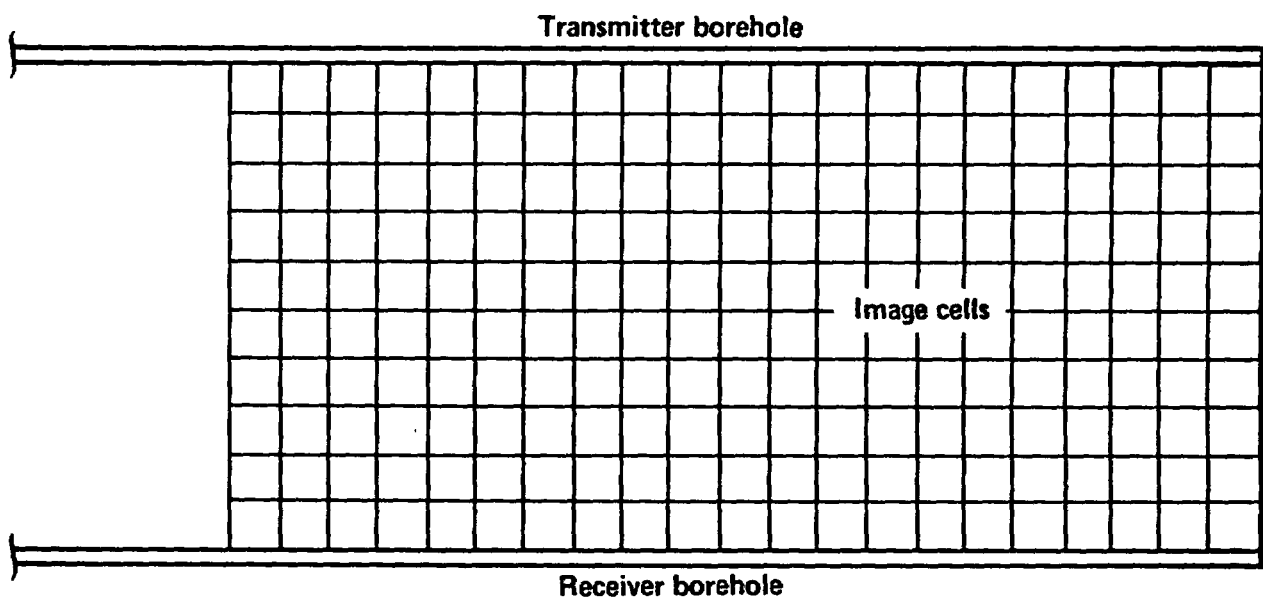


Figure A-2. The image plane between the boreholes modeled by a series of cells or pixels. We modeled the image region by 210 square cells each 10 cm on a side as shown. Each cell is assigned a uniform electromagnetic permittivity by the reconstruction algorithm.

where Δs_{ijk} is the ray length of ray k through cell ij and it is understood that $\Delta s_{ijk} = 0$ for all i and j not intercepted by a ray. Solution of Eq. 2A poses several problems. First the data t_k are necessarily inexact because of data noise which generally will make Eq. 2A inconsistent. Second, the number of independent equations can be insufficient so that the equations are underdetermined. Third, usually the number of equations is too large to be solved by direct inversion methods. In our case there are 10×21 cells or 210 unknowns and 441 rays.

Iterative methods, especially suitable for computer attack, have been devised which work well on underdetermined and inconsistent data. We have used the simultaneous iterative reconstruction technique (SIRT). It begins with an initial guess of v_{ij} and calculates an estimate for the data t_k . Then the difference between the data and calculated set is distributed along the ray paths. This leads to corrections in the estimated velocity function which, when applied, bring the estimate closer to the desired function. This process is repeated ray by ray and each cell is updated after all rays passing through a cell are considered. Ideally, these iterations continue until changes in the calculated t_k are of the order of the data noise. The algorithm is described in detail by Dines and Lytle (1979). The resultant image of 10×21 pixels is then smoothed using a linear interpolation algorithm which averages over an effective length of about one cell dimension but produces an image with 9 times the number of cells actually used in reconstruction.

APPENDIX B

Test Pit Experiment

An experiment was conducted in a sand test pit to simulate under controlled conditions some of the changes in moisture content which may develop around a heater in welded tuff. The primary objectives of this experiment were to 1) determine how accurately tomography images represent the shape and location of drying and wetting regions within a rock mass, 2) evaluate the validity of some of the assumptions and approximations used to solve the inverse problem and 3) test the measurement system and its sensitivity to changes in moisture content prior to field deployment.

The test pit was excavated in the shape of a cube with sides 2.5 m long and filled with moist sand that electromagnetically approximates partially saturated welded tuff. Figure B-1 shows a schematic diagram of the sand test pit and the simulated targets: a zone of dehydration intersected by a fracture. The simulated zone of dehydration was constructed using dry sand encased in impermeable plastic sacks. These sacks were fitted with plastic tubing so that water could be added to the sacks from the surface. The simulated fracture shown in Fig. B-1 was constructed using terry cloth and canvas encased in a plastic bag. It was also connected to the surface with plastic tubing so that water could be added.

Measurements of the real and imaginary parts of the complex dielectric constant were made as the moisture content of the simulated fracture and the dry sand region were changed. Figure B-2 shows the sequence followed in varying the moisture content. Measurements were made before step "a", between

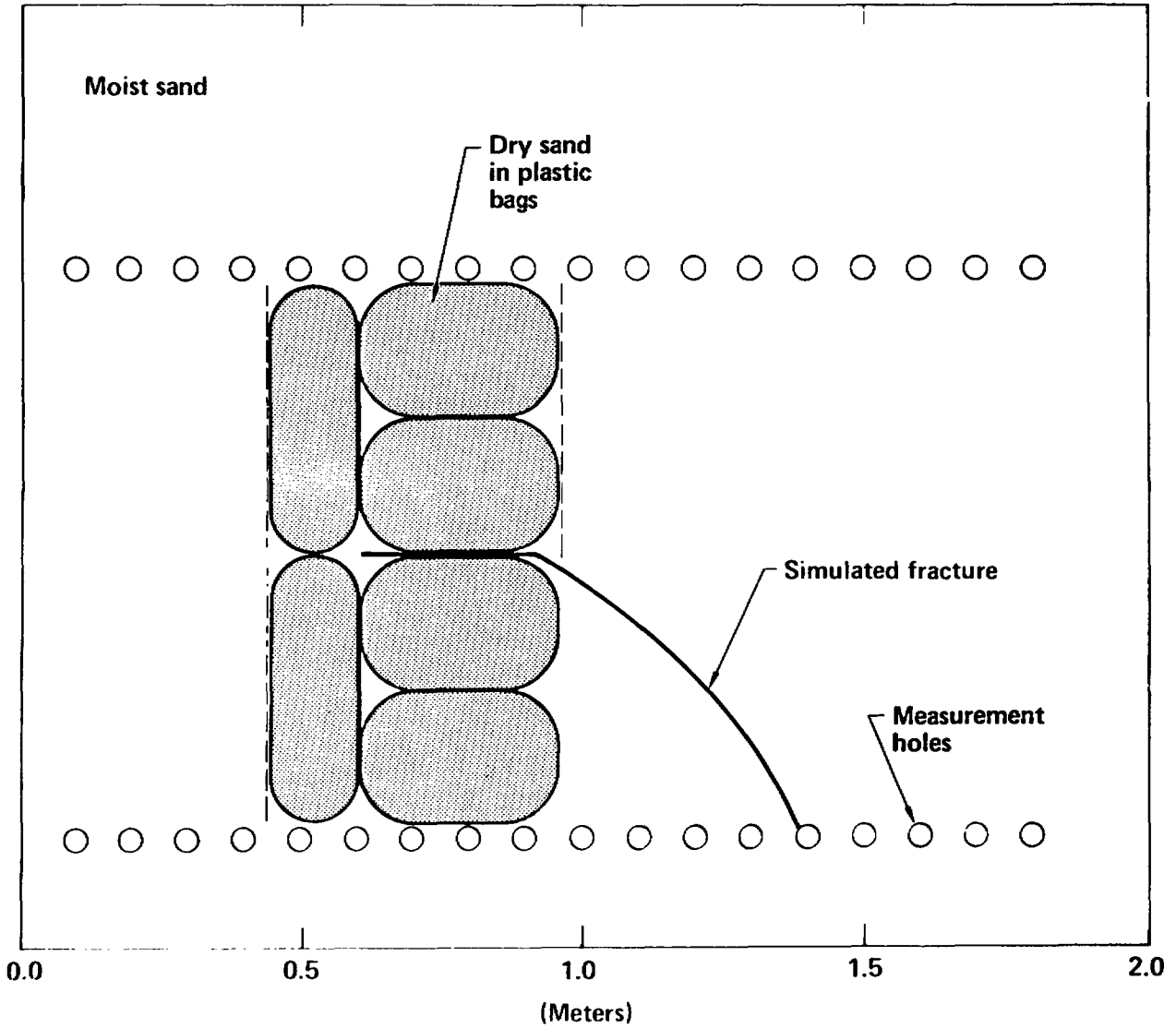


Figure B-1. Schematic diagram of the plan view for sand test pit and a zone of simulated dehydration intersected by a simulated fracture.

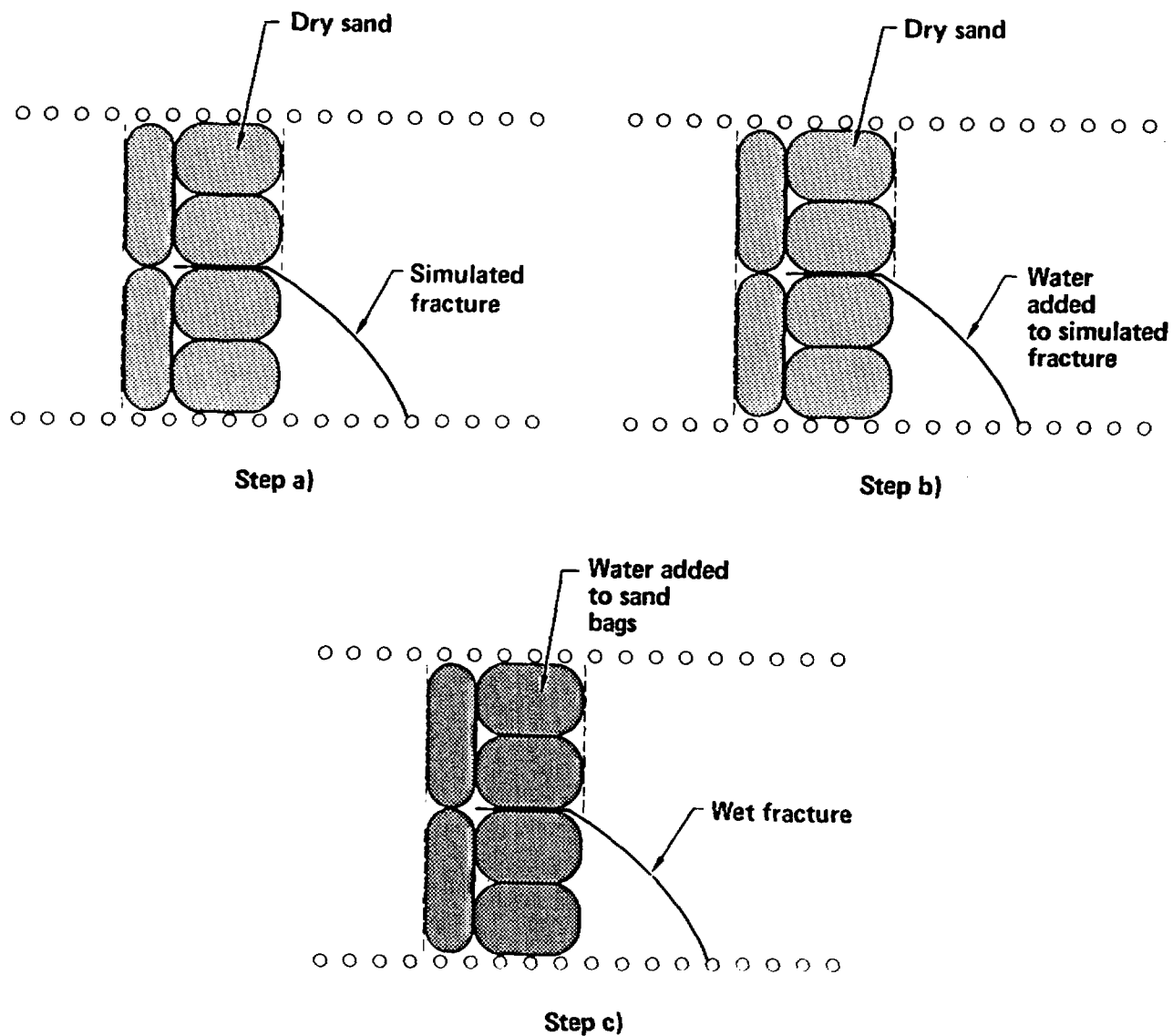


Figure B-2. Sequence followed in varying the moisture content of the targets embedded in the sand. Measurements were made before, during and after each change in moisture content was completed.

steps "a" and "b" and steps "b" and "c", and after step "c". Step "a" simulates welded tuff when a zone of dehydration has developed around the emplacement borehole and along a fracture. Step "b" simulates a zone of dehydration around the emplacement borehole and rewetting of the fracture caused by steam condensation. Step "c" roughly approximates the "natural" conditions prior to thermal loading where the rock around the emplacement borehole and around the fracture are at ambient conditions.

A set of measurements of phase and signal amplitude were made before and after each change in moisture content created in the test bed. Figure B-3 shows the results of measurements along parallel rays oriented orthogonal to the line of boreholes shown in Fig. B-1. The measurements shown were made when the sand bags and the simulated fracture were dry. Two basic trends can be observed in this figure: 1) Both the signal level and the real relative permittivity reach minimum values where the sand is dry and larger values where the sand is moist. Also, the contrast for both measurements is large enough such that the change is readily detectable. 2) The data shows oscillatory behavior on either side of the dry sand region. This may be indicative of interference phenomena. Possible sources for this phenomena are scattering from the large contrast and sharp boundaries in electromagnetic properties, or modes propagating parallel to the borehole axis because the wave length (~ 11 cm) is approximately a borehole diameter; this latter phenomena was observed and had to be corrected at G-tunnel when the ratio of wavelength to borehole diameter was of the same order.

Figure B-4 shows the results of the same ray paths after water was added to the dry sand bags. As expected, the permittivity increased in the region

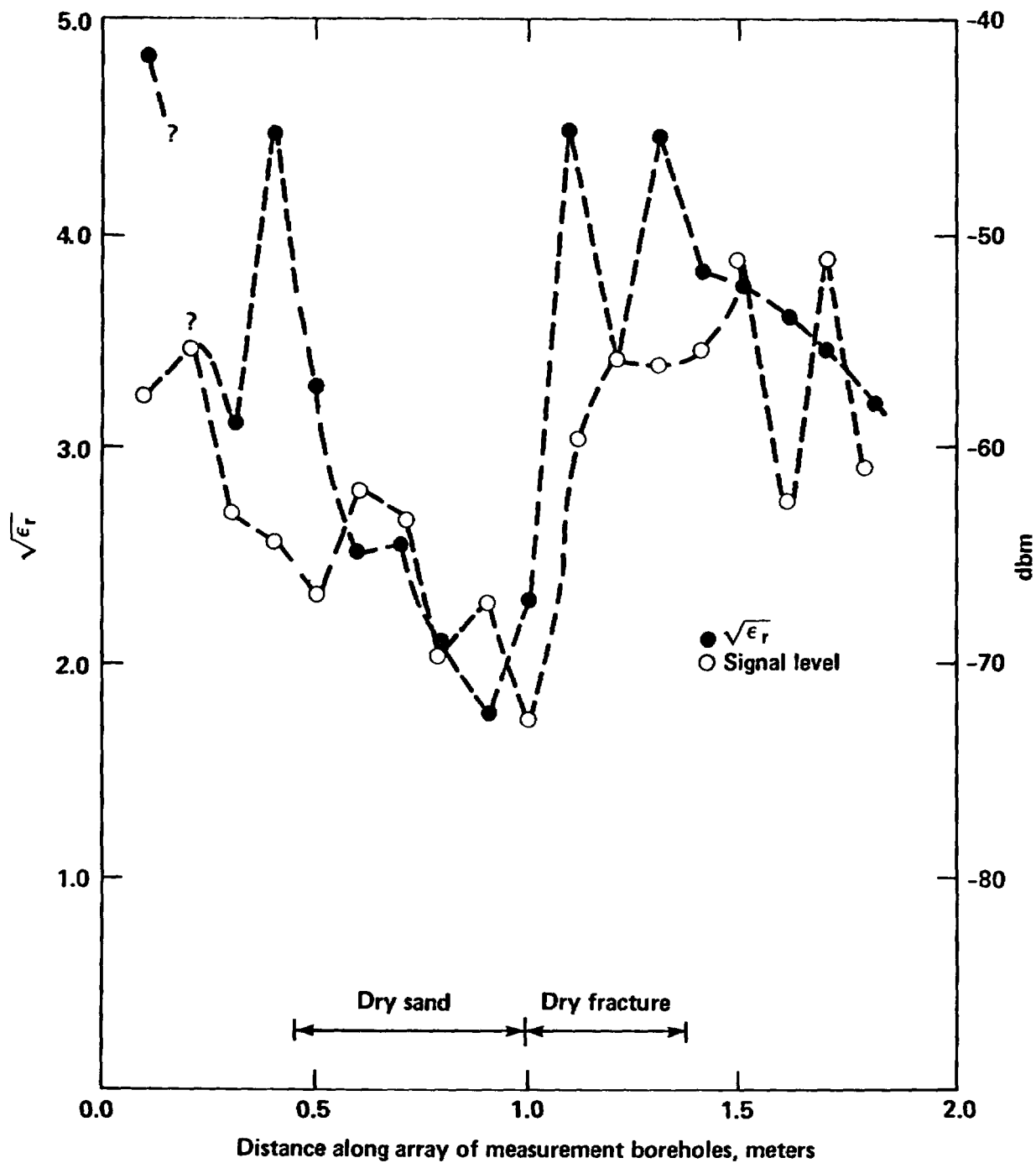


Figure B-3. Measurements of relative permittivity and signal amplitude made along parallel rays oriented orthogonal to the line of boreholes. The sand bags were dry during these measurements. Question marks indicate missing data.

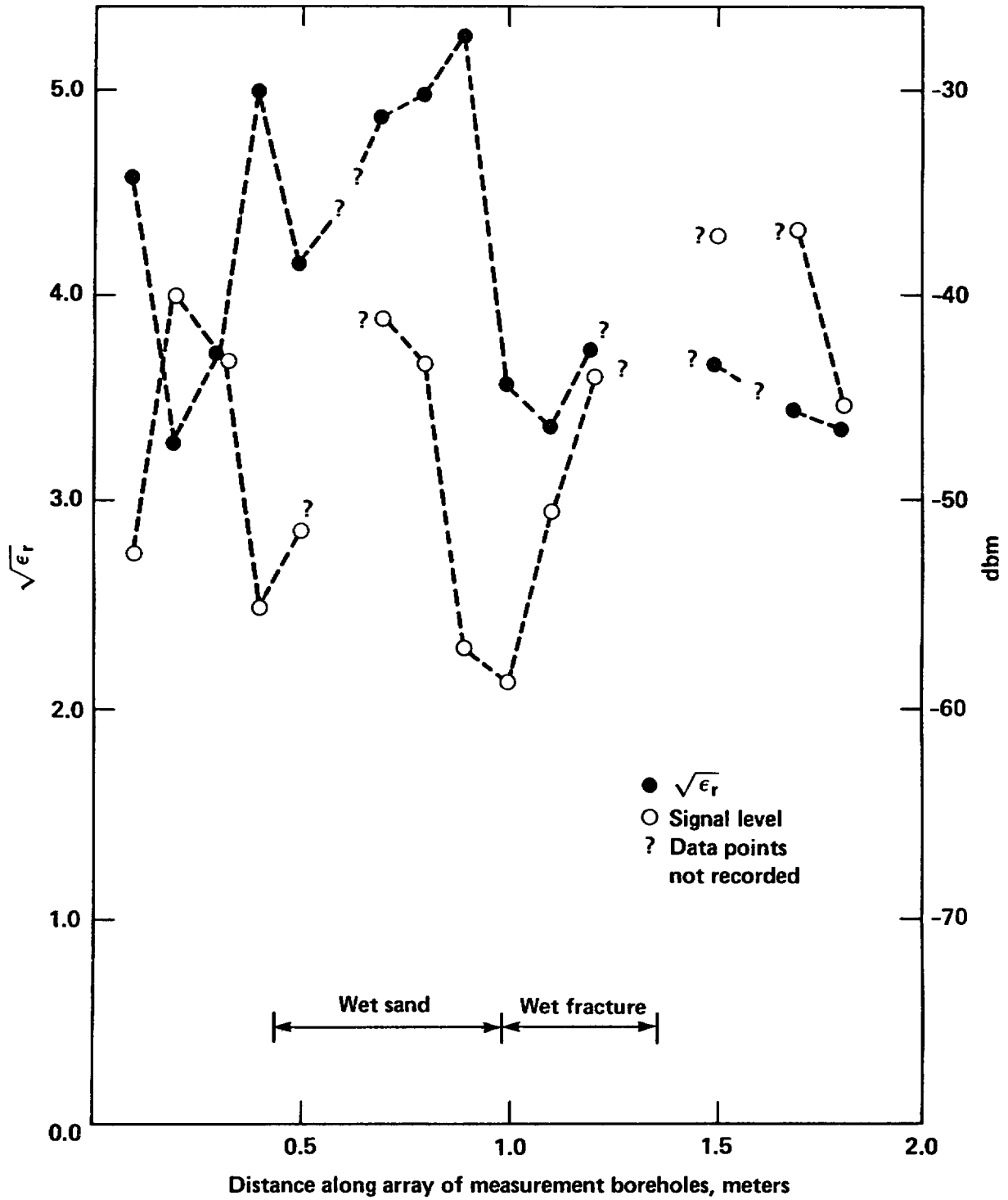


Figure B-4. Measurements of permittivity and signal amplitude made along parallel rays oriented orthogonal to the line of boreholes. Water was added to the sand bags in this case. Question marks indicate missing data.

of the sand bags. The oscillatory pattern observed when the sand bags were dry is still present. Also, the signal level measurements increased after fresh water was added to the sand bags. This was somewhat surprising in light of previous results which generally indicated an increase in attenuation factor as water content increased (Daily and Ramirez, 1984; Ramirez and Daily, 1985). When displacement currents dominate conduction currents, the electromagnetic attenuation rate is

$$\alpha = \frac{\sigma}{2} \left(\frac{\mu}{\epsilon_r} \right)^{1/2}$$

where

α = attenuation factor, the inverse skin depth

σ = electrical conductivity

ϵ_r = real part of the permittivity

μ = magnetic permeability

In many geologic environments the conductivity of the water is greater than the conductivity of the silicate matrix. Thus, as the moisture content increases, the effective rock mass conductivity (σ) increases and so does the attenuation factor. However, in some geologic environments, the groundwater has few dissolved solids such that the water conductivity is of the same order or less than the rock matrix conductivity. Changes in moisture content in these cases do not substantially change the effective rock conductivity (σ). However, the effective rock mass permittivity ϵ_r increases with moisture content thereby decreasing α . Thus, it is clear that α can increase or

decrease with increasing moisture content depending on the relative conductivities of the water and rock silicate matrix. When the electrical conductivity of the water relative to dry rock are unknown, or where it changes with time, measurements of attenuation factor can be misleading as an indicator of moisture content.

The electromagnetic measurements in the sand pit were inverted to form tomographs. Then the appropriate tomographs were subtracted from each other pixel by pixel. The resulting alterant tomographs should show locations within the test bed where the moisture content changed.

Figure B-5 is an alterant tomograph representing the changes relative in permittivity caused by adding water to the sand bags. The largest changes observed are at the position of the sand bags. However, some changes are also present in sections of the test pit where the moisture content should have remained constant. These changes are much greater than what could be explained based on measurement imprecision (see Results and Discussion section above). They likely result from the limited view distortion discussed above in Rockmass Heating.

Figure B-6 is an alterant tomograph representing the changes in relative permittivity caused by adding water to the simulated fracture. In this case, a discontinuous anomaly can be observed in the vicinity of the simulated fracture. However, other anomalies can be observed parallel to the simulated fracture. A likely explanation for this pattern is the limited view distortion.

There are some significant differences between the test pit anomalies and those encountered in welded tuff. A) The boundaries between the moist and dry

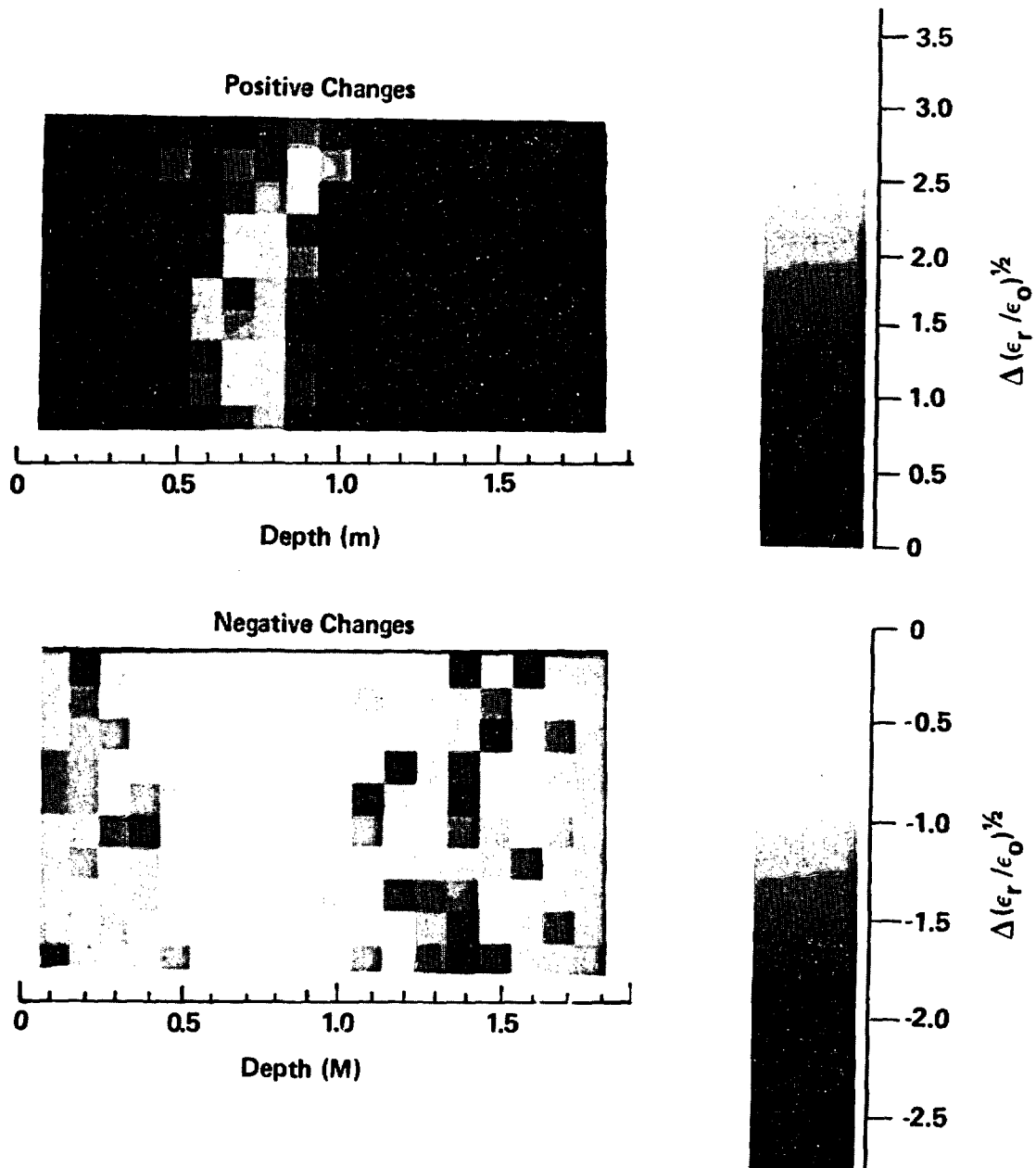


Figure B-5. Alterant tomograph (no spatial smoothing) representing the changes in relative permittivity caused by adding water the sand bags. Positive and negative changes are presented on the top and bottom images respectively.

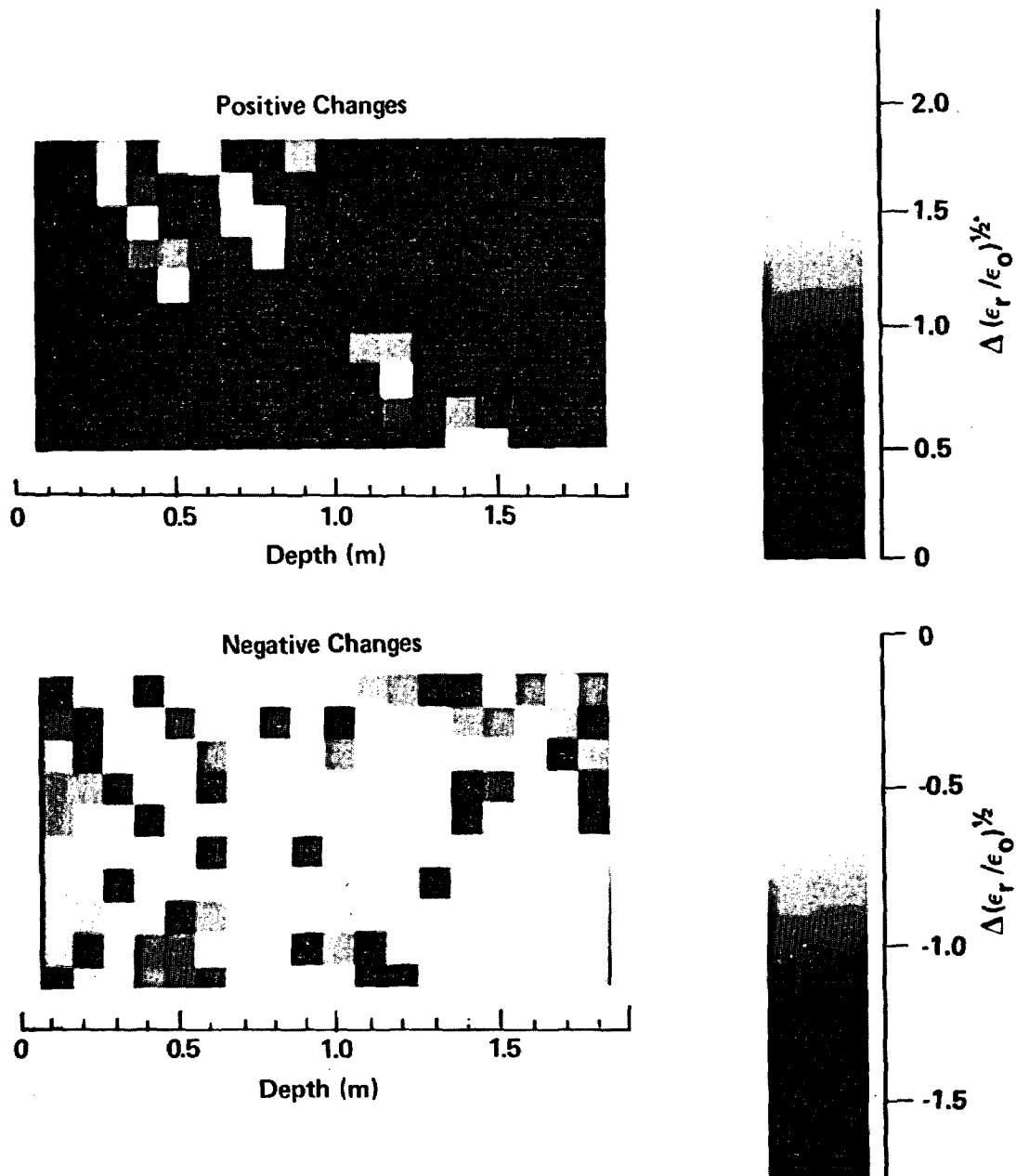


Figure B-6. Alterant tomograph (no spatial smoothing) representing the changes in relative permittivity caused by adding water to the simulated fracture. Positive and negative changes are shown by the top and bottom images respectively.

sand of the test pit are very abrupt whereas in welded tuff this transition in moisture content may occur over a distance of roughly 0.5 m (Nitao, 1986, personal communication). The abrupt transition in the moisture content of the test bed will result in more severe scattering behavior than from an anomaly in the rock. B) The width of the simulated wet fracture for case b (Fig. B-2) is substantially less than the analogous situation in welded tuff. Condensed water along a natural fracture may move into the matrix due to capillary suction. This would make the electromagnetic anomaly associated with the fracture several times wider and thus, easier to detect than the simulated fracture of the test bed. C) In the test pit the electric field polarization was fixed relative to the anomaly orientation in the sand. In a natural environment of highly fractured tuff, signal polarization will probably not be similar to all targets of interest in the rock mass. Since details of the interaction between the signal polarization and target orientation will vary, it may be difficult to compare test pit results to in situ results in tuff.

Several sets of high frequency electromagnetic measurements were conducted within the sand test bed. Various targets embedded within the bed roughly approximated some of the changes in moisture content that may develop around a heater in welded tuff. Three lessons were learned as a result of this experiment:

1. Changes in water content created within the simulated dehydration regions were readily detectable. Also detected were other apparent changes scattered at various locations throughout the sand matrix. Similarly, the changes in location along the simulated fracture were also detected. In addition, other anomalies were observed approximately parallel to the simulated fracture.

2. Our judgment is that the changes observed away from locations where the moisture content was changed can be explained by one or more of the following factors: 1) The contrasts in wave velocity are large enough to make the straight-ray approximation invalid in this case. This phenomenon could also account for the anomalies observed to develop parallel to the simulated fracture. 2) Wave scattering could also have occurred along the dry sand/moist sand boundaries or due to reflections from a water table which formed just below the plane of measurement. 3) There are also indications that the moisture content of the sand surrounding the targets may have changed during the experiments, probably due to drainage through the sand. This adds a degree of uncertainty to the interpretation of the results. 4) Sampling with rays between points on only 2 sides of the target results in image artifacts which we have referred to above as limited view distortions.
3. The diagnostic value of permittivity for moisture content determination was clarified by this experiment. In fact we found that permittivity is, in many cases, a better diagnostic to changes in moisture than attenuation rate measurements. Permittivity always increases with increasing moisture content; attenuation factor, on the other hand, can increase or decrease (depending on the electrical conductivity of the water) with increasing moisture content and thus, can be an ambiguous diagnostic.

ACKNOWLEDGMENTS*

The authors gratefully acknowledge assistance from many colleagues at LLNL during the course of this work. S. Rupert spent many weeks processing the field data and R. Egbert was very helpful in fielding the experiment. J. Berryman, N. Burkhard, T. Buscheck, E. Laine, P. Kasameyer, D. Wilder and J. Yow, Jr. made many helpful suggestions during the experiment and during the preparation of this manuscript. M. Buettner and J. Beatty provided invaluable computer and instrumentation support. Many helped during data acquisition in the field including J. Beatty, J. Berryman, J. Carbino, G. Holladay, E. Owen and H. Wang.

The G-Tunnel experiment was made possible by the generous cooperation of employees of Sandia National Laboratories. R. Zimmerman made available the experimental site and provided guidance in planning the experiment. J. Bradshaw and R. Schuch provided varied invaluable support during execution of the experiment.

REFERENCES

Burkhard, N. R., "Resolution and Error of the Back Projection Technique Algorithm for Geophysical Tomography," Lawrence Livermore National Laboratory, UCRL-52984, 1980.

* Work performed under the auspices of the U.S. Department of Energy by the Lawrence Livermore National Laboratory under contract number W-7405-ENG-48.

Daily, W. D., W. Lin and T. Buscheck, "Hydrological Properties of Topopah Spring Tuff -- Laboratory Measurements," J. Geophysical Res., in press, 1987.

Daily, W. D. and A. L. Ramirez, "In-Situ Porosity Distribution Using Geophysical Tomography," Geophy. Res. Letts., 11, No. 6, 614-616, 1984.

Dines, K. A. and R. J. Lytle, "Computerized Geophysical Tomography," Proc. IEEE, 67, No. 7, 1065-1073, 1979.

Eisenberg, D. and W. Kauzmann, The Structure and Properties of Water, Oxford University Press, New York, 1969.

Freeman, M. S., R. N. Nottenburg and J. B. DuBow, "An Automatic Frequency Domain Technique for Dielectric Spectroscopy of Materials," Inst. Phys. E: Sci. Instrum., 12, 1-5, 1979.

Hearst, J. R. and P. A. Nelson, Well Logging for Physical Properties, McGraw Hill Book Company, 1985.

Johnstone, K. J. and K. Wolfsberg (eds.), "Evaluation of Tuff as a Medium for Nuclear Waste Repository: Interim Status Report on the Properties of Tuff," Sandia National Laboratory, SAND 80-1464, Albuquerque, New Mexico, 1980.

Jordan, E. L., (ed.), Reference Data for Engineers: Radio, Electronics, Computer, and Communications, 7th Edition, Howard Sams and Co., Indianapolis, 1985.

Kuhl, D. E. and R. O. Edwards, "Image Separation Radioisotope Scanning," Radiology, 80, No. 4, 653-662, 1963.

Lager, D. L. and R. J. Lytle, "Determining a Subsurface Electromagnetic Profile from High-Frequency Measurements by Applying Reconstruction Technique Algorithms," Radio Science, 12, No. 2, 249-260, 1977.

Langkopf, B. S. and E. Eshom, "Site Exploration for Rock Mechanics Field Tests in the Grouse Canyon Member, Belted Range Tuff, U12g Tunnel Complex, Nevada Test Site," Sandia National Laboratories, SAND 81-1897, Albuquerque, NM, 1982.

Lytle, R. J. and K. A. Dines, "Iterative Ray Tracing Between Boreholes for Underground Image Reconstruction," IEEE Trans. on Geoscience and Remote Sensing, GE-18, No. 3, 234-240, 1980.

Meador, R. A. and P. T. Cox, "Dielectric Constant Logging: A salinity independent estimation of formation water volume," SPE Paper 5504, 50th Annual Fall Mtg., 1975.

Menke, W., "The Resolving Power of Cross-Borehole Tomography," G. Res. Letters, 11, No. 2, 105-108, 1984.

Poley, J. Ph., J. J. Nootboom, and P. J. deWaal, "Use of VHF Dielectric Measurements for Borehole Formation Analysis," Log Analyst, May-June, 8-30, 1978.

Ramirez, A. L., "Reconstruction of Simulated Lineaments Using Geophysical Tomography," Intl. J. of Rock Mech. & Min. Sci. and Geo-Mech. Abs., 23, No. 2, pp. 157-163, 1986.

Ramirez, A. L. and R. J. Lytle, "Investigation of Fracture Flow Paths Using Alterant Geophysical Tomography," Intl. J. Rock Mech. Min. Sci. and Geomech. Abstr., 23, No. 2, pp. 165-169, 1986.

Ramirez, A. L. and W. D. Daily, "Evaluation of Alterant Geophysical Tomography in Welded Tuff," J. Geophys. Res., in press, 1987.

Von Hippel, A. R. (Ed.), "Dielectric Materials and Applications," The Technology Press of M.I.T. and John Wiley and Sons, New York, 1954.

Winograd, G. J. and W. Thordarson, "Hydrologic and Hydrochemical Framework," Hydrology of Nuclear Test Sites, U.S. Geological Survey, Professional Paper 712-C, 1975.

Zimmerman, R. M. and M. B. Blanford, 1986, "Expected Thermal and Hydrothermal Environments for Waste Emplacement Holes Based on G-Tunnel Heater Experiments," Proc. 27th Symposium on Rock Mechanics, Chapter 125, pp. 874-882, 1986.

Zimmerman, R. M., M. B., Blanford, J. F. Holland, R. L. Schuch, and W. H. Barrett, "Final Report, G-Tunnel Small Diameter Heater Experiments," SAND84-2621, Sandia National Laboratories, Albuquerque, NM, 1984.

Zimmerman, R. M., F. B. Nimick, and M. B. Board, 1984, "Geoengineering Characterization of Welded Tuffs from Laboratory and Field Investigations," Proceedings of 1984 Symposium on Scientific Basis for Nuclear Waste Management VIII, Materials Research Society, Boston, MA.

Technical Information Department · Lawrence Livermore National Laboratory
University of California · Livermore, California 94550

